McGill University

Chemical Engineering

Faculty of Engineering

Université McGill

Génie Chimique

Faculté de Génie

Optimisation and characterization of a novel microchannel emulsification process for pancreatic beta cell microencapsulation in alginate

Christina Bitar

Department of Chemical Engineering

McGill University, Montreal

December 2018

A thesis submitted to McGill University in partial fulfillment of the requirements of the degree of Master of Engineering

Abstract

The transplantation of encapsulated islets has the potential to provide a long-term treatment for type 1 diabetes while avoiding the need for chronic immunosuppression required for current islet transplants. Conventional encapsulation techniques using nozzles have limited throughput and produce beads that are permeable to immune system components such as antibodies. Islet encapsulation in alginate beads by stirred emulsification and internal gelation can overcome these limitations but generates beads with a broad size distribution. Microchannel emulsification is a versatile approach for the scalable production of oil-in-water (O/W) or water-in-oil (W/O) microdroplets of uniform size. In this study, microchannel emulsification technologies were employed to produce alginate droplets in an oil phase (W/O emulsion). This process was combined with the internal gelation of alginate to introduce a novel microchannel emulsification cell encapsulation bioprocess to the field of cellular therapy. The initial microchannel emulsification prototype was improved by selecting 3M™ Novec™ 7500 Engineered Fluid as the continuous oil phase and polytetrafluoroethylene as the microchannel plate material to achieve the spontaneous generation of monodisperse alginate microbeads ranging from ~1.5 to 2.5 mm in diameter at production rates exceeding 140 mL/h per microchannel. The beads produced using this device were more uniform in size than beads obtained by stirred emulsification, in addition to demonstrating enhanced compressive burst strength and more uniform pore size distribution based on inverse size exclusion chromatography. Although further process optimization is required to improve encapsulated cell survival, the microchannel emulsification device is a promising alternative technique for the successful immunoisolation of pancreatic islet cells for diabetes cellular therapy. The microchannel emulsification process could also be adapted to other encapsulation applications in the pharmaceutical, food, agriculture and cosmetic industries.

Résumé

En créant une barrière immunoprotectrice, l'encapsulation d'îlots pourrait mener à un traitement durable au diabète de type 1 tout en évitant le recours aux médicaments immunosuppresseurs présentement requis pour éviter le rejet de greffes d'îlots. Les techniques d'encapsulation par buse conventionnelles ont des taux de production limités et forment des billes qui sont perméables à certaines composantes du système immunitaire comme les anticorps. Une méthode basée sur l'émulsion de l'alginate sous agitation dans une phase organique a été proposée plus récemment afin de surmonter ces limitations, mais ce procédé génère des billes avec une large distribution de taille. L'émulsification par microcanaux est une approche polyvalente pour la production de microgouttelettes uniformes d'huile dans l'eau (H/E) ou d'eau dans l'huile (E/H). Dans cette étude, des technologies d'émulsification par microcanaux ont été utilisées pour produire des gouttelettes d'alginate dans une phase organique (émulsion E/H). Ce procédé a été combiné avec la gélification interne de l'alginate pour introduire un nouveau bioprocédé d'encapsulation cellulaire grâce à l'émulsification par microcanaux dans le domaine de la thérapie cellulaire. Le prototype initial d'émulsification par microcanaux a été amélioré en choisissant le fluide 3M™ Novec™ 7500 Engineered Fluid comme phase huileuse continue et le polytétrafluoroéthylène comme matériau de fabrication de la plaque à microcanaux pour permettre la génération spontanée de microbilles d'alginate monodispersées allant d'environ 1,5 à 2,5 mm de diamètre à des débits de production supérieurs à 140 ml/h par microcanal. Les billes produites à l'aide de ce dispositif avaient une taille plus uniforme que les billes obtenues par émulsification sous agitation, en plus de démontrer une résistance à l'éclatement sous compression améliorée et une distribution plus uniforme de la taille des pores basée sur la chromatographie d'exclusion de taille en phase inverse. Bien qu'une optimisation supplémentaire du processus soit nécessaire pour améliorer la survie des cellules encapsulées, le dispositif d'émulsification par microcanaux est une technique alternative prometteuse pour l'immunoisolation des cellules d'îlots pancréatiques pour la thérapie cellulaire du diabète. Ce procédé d'émulsification par microcanaux pourrait aussi être adapté à d'autres applications d'encapsulation dans les industries pharmaceutique, alimentaire, agricole et cosmétique.

Acknowledgments

I would first like to thank my supervisor, Dr. Corinne Hoesli, for your guidance throughout the project, as well as your motivation and inspiration to becoming a better researcher. I could not have asked for a better voice of reason throughout my project.

Secondly, I owe a huge thanks to the entire Hoesli lab for making long hours in the lab enjoyable. Lisa, Mohamed, Ray, Stephanie, and Ariane: thank you for training me on various laboratory equipment and procedures. Brenden and John: thank you for sharing my passion for all things encapsulation-related, and for being great lab bench mates. Thank you, Karen, for training me on how to use a biosafety cabinet for the first time and providing me a good head start on my project. Gad, thank you for helping me with trouble-shooting, and teaching me to become a better researcher overall. Thank you to my undergraduate summer students, Chloé and Zhiqing, for lending a helping hand when needed.

Thank you to Igor Lacík, Dušana Treľová, and Zuzana Kroneková for conducting the mechanical characterizations of my microchannel and stirred emulsification microbeads (compression tests, inverse size exclusion chromatography, and Raman spectroscopy). James Dietrich, thank you for laser micromilling my microchannel plates, and for training me on how to use the laser micromill. Big thanks to Galyna Shul (surface tension measurements) and Ranjan Roy (contact angle measurements) for technical support. This project was funded by Natural Sciences and Engineering Research Council of Canada, Montreal Diabetes Research Center, Diabète Québec, Fonds de recherche sur la nature et les technologies, Quebec Network for Cell, Tissue and Gene Therapy – ThéCell (a thematic network supported by the Fonds de recherche du Québec-Santé), Juvenile Diabetes Research Foundation, and PROTEO.

Finally, I would like to thank my parents for keeping me well fed during my trips to Ottawa, and constantly encouraging me to achieve my full potential. Andrew, thank you for being the best role model I could ask for. I can only hope to continue following in your footsteps. Matthew, thank you for your unconditional love and support, and I look forward to what you will have to offer in the near future.

Table of Contents

List of Figures

List of Tables

Statement of Contribution

The initial microchannel emulsification prototype was previously designed by Karen Marwick in the Stem Cell Bioprocessing Lab at McGill University (Montreal, Canada). I conducted all optimization and characterization experiments outlined in the materials/methods and results sections in the same laboratory with the following exceptions:

1) Chloé Selerier, an undergraduate summer student intern, conducted the viscosity and surface tension measurements for the alginate and continuous phase fluids. Viscosity measurements were conducted using a rheometer shared by the labs of Prof. Richard Leask and Prof. Milan Maric at McGill University. The surface tension measurements were done using a dynamic tensiometer found at l'Université de Québec à Montréal with the assistance of Galyna Shul.
2) Inverse size exclusion chromatography, texture analysis, and Raman spectroscopy measurements were conducted by Igor Lacík, Dušana Treľová, and Zuzana Kroneková at the Polymer Institute of Slovak Academy of Sciences, Department for Biomaterial Research (Bratislava, Slovakia). I prepared the microchannel and stirred emulsification microbeads at McGill University and shipped them to Slovakia for analysis. Figure 16 and Figure 18 were produced by Igor, Dušana and Zuzana, and I participated in the interpretation of these results.

1 Introduction

Bioencapsulation involves coating active substances with a semipermeable material to provide protection, immobilization, controlled release, and/or improved functionality of active components [1]. A common application of bioencapsulation in cellular therapy is the immobilization and transplantation of donor insulin-producing pancreatic islet cells as a type 1 diabetes treatment option. Type 1 diabetes is a chronic illness in which the body undergoes an autoimmune response against pancreatic beta cells, decreasing the production of insulin, a necessary hormone for glucose regulation in the body. Insulin promotes glucose uptake in the liver, muscle and fat cells to be used for energy or to be stored as glycogen (Figure 1). If left untreated, diabetes may lead to secondary complications including renal failure, blindness, or coronary and peripheral vascular-occlusive disease [2].

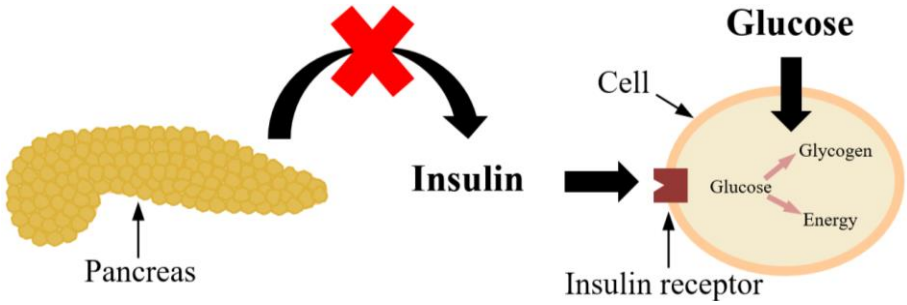

Figure 1. Schematic representation of type 1 diabetes.

The conventional treatment for type 1 diabetes comprises regular blood sugar monitoring, exogenous insulin administration, carefully controlled diet and exercise. However, this method of treatment has a negative impact on patient quality of life as it may lead to pain and bruising and can be considered a serious burden. Moreover, blood glucose variations occur as insulin injections fail to achieve tight glucose control, leading to increased risk of severe hypoglycemic events and potential long-term complications [3, 4]. Insulin pumps with glucose sensors have removed the daily burden of insulin injections while providing enhanced blood glucose regulation [5]; however, pumps carry the inconvenience of carrying an external device that requires monitoring and user input. To successfully treat type 1 diabetes, glucose control should be achieved through an internal closed-loop system configuration with minimal patient input and monitoring, similarly to non-diabetics. This may be achieved by replacing insulin-producing cells in diabetic patients with pancreatic islet transplants [4].

Allogeneic islet transplantation is a promising alternative treatment of type 1 diabetes [6, 7]. It is much less invasive than whole pancreas transplantation, which requires longer recovery times [6]. The Edmonton Protocol (2001) was the first promising islet transplantation method by which insulin independence could be achieved in most patients for ~1 year [8]. Since then, this treatment has been able to achieve sustained exogenous insulin independence in 50% to 70% of patients for 5 years [9]. However, the subsequent immune rejection of unprotected transplanted islets is almost inevitable without the lifelong use of immunosuppressive drugs that may lead to severe side-effects such as opportunistic infection and cancer [2]. Furthermore, this treatment is not available to all patients due to limited donor supply [10].

Islet cell encapsulation in hydrogels, illustrated in Figure 2, has been extensively studied to protect transplanted islets against the immune system components that attack foreign matter through the body's defence mechanism [2]. The porous encapsulation material should selectively prevent the entrance of immune cells and potentially antibodies, while permitting the diffusion of oxygen, nutrients and insulin. Encapsulation technologies should therefore reduce the need for immunosuppression and expand the available donor beta cell supply by including allogeneic, xenogeneic and pluripotent stem cells [10-12].

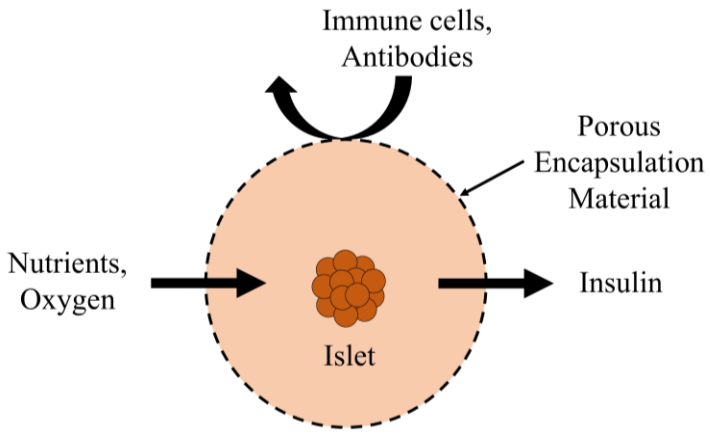

Figure 2. Schematic representation of pancreatic islet cell microencapsulation. The porous encapsulation material (e.g. alginate hydrogel) acts as a size exclusion barrier to protect the graft from host immune cells and potentially antibodies upon implantation, without the requirement of immunosuppression.

Islets can either be enclosed within macrocapsules or microcapsules and introduced into the body at various potential sites such as the peritoneal cavity, subcutaneous sites or under the

renal capsule [10]. Macroencapsulation involves the use of a single encapsulation device immobilizing several islets. The major drawback associated with this technique is the limited oxygen supply resulting in central necrosis of islets [10]. Additionally, if the integrity of the macroencapsulation device is compromised, graft rejection may result. Alternatively, microencapsulation involves the individual encapsulation of islets in several microspheres. This configuration is attractive due to the increase in surface area to volume ratio of microcapsules, reducing oxygen diffusion limitations. Microencapsulation also requires less complex manufacturing processes and less invasive surgery than macroencapsulation [10].

Encapsulation of cells within spherical alginate microcapsules is one of the most broadly investigated immunoisolation methods in cellular therapy. Ideally, alginate microbeads should be monodisperse at diameters between 600 µm and 800 µm to minimize oxygen diffusion limitations, while ensuring complete islet encapsulation [12, 13]. Production rates of beads that each encapsulate one islet should reach approximately 100 mL in less than 1 hour, to be able to treat one patient within a reasonable timeframe. Moreover, bead production processes that can operate at high fluid viscosities are desirable since higher alginate viscosities associated with higher polymer concentration can enable the production of beads impermeable to antibodies without the necessity of exterior polymer coatings. It was previously found that alginate concentrations of 5% (~3 Pa·s) were sufficient to avoid antibody access to most of the gel volume [14, 15]. Current devices are either limited in the viscosity range, production rate or bead uniformity. There is a need for more research in the development of a novel device that can accommodate high alginate concentrations while leading to sufficient production rates of monodisperse alginate beads.

The Stem Cell Bioprocessing Lab (McGill University) has developed a preliminary microchannel emulsification prototype that can produce relatively monodisperse (variation of <10%) alginate microbeads of approximately 3 - 5 mm in diameter, at a production rate of 4 mL/min/channel [16]. Further improvements to the microchannel emulsification process design is required to achieve the target diameter, production rates and uniformity. Ultimately, this should bring research one step closer to long-term insulin independence in type 1 diabetic patients using microencapsulated islet transplantation.

2 Literature Review

Islet immobilization in alginate has the potential to eliminate the two major problems associated with islet transplantation as a long-term type 1 diabetes treatment option: limited donor supply and lifelong administration of immunosuppressive drugs. Progress in macroencapsulation device development has included improved oxygen supply to immobilized islets (e.g. Beta-O_2 device) [17, 18], the development of planar pouch devices designed for subcutaneous implantation (e.g. ViaCyte devices) [19], and the use of pro-angiogenic factors for enhanced vascularization, such as the infusion of vascular endothelial growth factor into the TheraCyte device [20]. However, macroencapsulation devices are intrinsically limited in the accessible surface area to volume ratio for mass transfer compared to microencapsulation. Microbeads have been shown to be durable and require minimal surgery [21]. Furthermore, the beads can be separated and implanted into various sites in the body including the peritoneal cavity, under the renal capsule, or subcutaneously [10, 21]. For these reasons, this work focusses on the potential of microencapsulation to successfully immunoisolate insulin-producing pancreatic beta cells in a scalable and effective manner.

The following sections provide a detailed literature review of alginate as a microencapsulation material, microencapsulation methods, transplantation of microencapsulated islets, the mechanism of droplet formation in microchannel emulsification, microbead characterization methods and cell viability assessment techniques.

2.1 Alginate as a Cell Microencapsulation Material

Microencapsulation materials must be carefully selected for the application of islet transplantation to ensure sufficient permeability for nutrients to enter and insulin to escape, long-term stability and biocompatibility. Several encapsulation materials have been investigated including polyethylene glycol [22], poly(lactic-*co*-glycolic acid) [23], agarose [24], polyacrylate [25] and alginate [26]. Hydrogels (e.g. alginate, agarose, chitosan, and polyethylene glycol) are the most commonly used encapsulation materials for drug and cell delivery systems due to their wetting properties and low immunogenicity [27]. Hydrogels are hydrophilic in nature, resulting in almost no interfacial tension with surrounding fluids and tissues, minimizing protein adsorption and adhesion of inflammatory cells secreting cytokines and chemokines that would negatively

influence the graft function. The growth of cells on the surface of microcapsules would also reduce oxygen and nutrient diffusion to the encapsulated graft, ultimately resulting in necrosis of the encapsulated cells. Furthermore, hydrogels are advantageous due to their soft and pliable nature, reducing mechanical or frictional irritations to encapsulated cells as well as the surrounding tissue [12].

Alginate, a naturally occurring biomaterial extracted from brown seaweed, is the most ubiquitously used hydrogel for islet encapsulation [4]. As shown in Figure 3, alginate molecules are anionic linear block co-polymers of varying chain length, consisting primarily of uronic acid units (α-(1-4)-L-guluronic and β-(1-4)-D-mannuronic acid) connected by 1:4 glycosidic linkages. The L-guluronic and D-mannuronic acid subunits are referred to as G and M subunits, respectively.

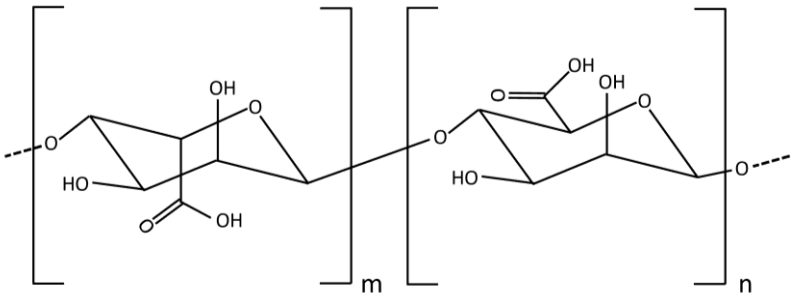

Figure 3. General structure of alginate polymer with uronic acid subunits.
Alginate is composed of various combinations of the two uronic acid subunits: α-(1-4)-L-guluronic acid (left) and β-(1-4)-D-mannuronic acid (right).

The process of islet microencapsulation in alginate involves the entrapment of islets in an alginate microdroplet, which undergoes ionotropic gelation in the presence of divalent cations (e.g. Ca^{2+} or Ba^{2+}), forming a gelled microbead. The regions in alginate that contribute to gel formation are mainly the G-blocks [28] with slight contribution from alternating M and G blocks (MG-blocks) [29]. Unlike M-blocks, these regions along alginate are able to form junctions for enhanced divalent cation binding [29].

To increase alginate bead strength and stability while reducing permeability, beads can be coated with a cationic polymer membrane (e.g. poly-L-lysine). Since cationic polymers lead to immunogenic responses, a second alginate layer can be added following the cationic polymer coating [30]. Furthermore, Ba^{2+} ions were shown to form stronger alginate gels with minimal

swelling due to their higher affinity towards alginate compared to Ca^{2+} ions, specifically for alginates with high-G content [28, 31-33]. The toxicity of free Ba^{2+} ions raises concerns in its use as a gelling agent [12]; however, strategies to avoid toxicity of this gelling cation include using a concentration below 5 mM [34] and eliminating any excess Ba^{2+} after the gelation process through rinsing and/or sulfate precipitation [30, 35]. Alternatively, adjustments to the chemical composition (M:G ratio and sequential arrangement) or molecular weight of the alginate polymer, as well as the kinetics of the gel-formation process, can have an impact on the long-term immunoprotection capacity, mechanical integrity, chemical stability, and cell-adherence propensity of the alginate-based microcapsules [2, 4].

A challenge associated with the use of alginate as an encapsulation material is the lot-to-lot variability in polymer length and composition associated with most natural polymers [12]. This leads to difficulties in controlling the properties and function of alginate as a material for islet encapsulation. A second challenge is that crude alginate contains toxic polyphenols, proteins, and endotoxins, which stimulate the immune system [36]. Purification of the crude alginate is therefore required prior to use as a transplantation material, to improve the biocompatibility of alginate-based microbeads. Typically, the endotoxin content in the purified alginate should be below 100 EU/g to be permitted during *in vivo* studies [12]. Furthermore, heat sterilization of alginate causes a decrease in molecular weight and viscosity of alginate due to depolymerization [37, 38]. However, controlling the pH at 7-8 with buffered solutions or adding a filler/nutrient to the solution was shown to inhibit the depolymerization reaction [39].

2.2 Cell Microencapsulation Methods

2.2.1 Nozzle-Based Encapsulation and External Gelation

Nozzle-based encapsulation and external gelation is a commonly used islet encapsulation technique involving alginate droplet formation at the tip of a nozzle, followed by external gelation when the droplet enters into contact with a solution containing divalent cations (typically Ca^{2+} or Ba^{2+}), as displayed in Figure 4.

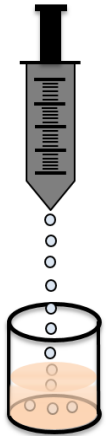

Figure 4. Nozzle-based extrusion and external gelation process for microbead production. Alginate is extruded at the nozzle tip forming droplets that are released into a $CaCl_2$ bath (or $BaCl_2$) and undergo external gelation.

In most nozzle-based encapsulators, droplet release is dictated by gravity, vibration, or electrostatic forces. The gelling cations (e.g. Ca^{2+} or Ba^{2+}) diffuse from the external solution into the droplet and interact with the carbonyl groups of the alginate blocks, creating a three-dimensional network in the form of a spherical microcapsule. The gravity-based nozzle encapsulation process produces droplets that detach only when the gravity force exerted on the droplet exceeds the upwards surface tension force. Droplet formation can be accelerated and droplet size can be reduced by obtaining a jet at the nozzle tip that is destabilized through electrostatic forces, vibration or physical cutting [40-42].

In electrostatic nozzle-based encapsulators, a suspension of islets in alginate solution passes through a needle charged with a potential typically ranging from 3 to 12 kV. A grounded divalent cation bath is placed close enough to the needle to allow for the formation of a stable electrical field, which draws droplets into the collection bath. The formation of small discrete droplets occurs through pulsation of the potential generated by a high voltage power source, at frequencies of approximately 40 Hz, in a square wave pattern [43]. The droplets achieved here are highly uniform. This process is cytocompatible, simple, and can be performed aseptically in a closed system. However, the scale-up potential of this process is limited, at maximum achievable production rates of approximately 60 mL/h [44, 45]. Scale-up would require the setup of several extrusion needles in parallel, increasing cost and complexity.

In vibrating nozzle encapsulation, the liquid flow rate can be increased to a point where liquid jetting occurs at the tip of the nozzle, and vibration is introduced to break up the liquid jet into discrete droplets [43]. Vibrating nozzle systems can produce small and narrowly distributed beads, approximately 0.3 to 5 mm in diameter [46]. However, this process is limited to fluids with viscosities lower than 200 mPa·s, since higher viscosity fluids result in vibration damping, which prevents the jet from breaking up into discrete droplets [43].

The JetCutter nozzle-based encapsulation method involves the cutting of a high velocity continuous fluid jet into segments by a rotating cutting tool. The segments become spherical in shape due to the surface tension forces as they fall into the collection bath. The bead size is easily adjustable by changing the rotating speed of the cutting tool. This technique accommodates higher fluid viscosities (up to several thousand mPa·s) than vibrating and electrostatic nozzle encapsulators [46]. Furthermore, very high throughputs are achievable using this technology (up to 2,000 mL/h) [46, 47]. However, the use of this technique in the encapsulation of primary islets has not yet been reported.

Although nozzle-based encapsulation is the most commonly used technique for islet microencapsulation due to its simplicity, it has several limitations that have provoked the development of alternative techniques to produce alginate microcapsules. These limitations include the limited alginate viscosity operating range, the risk of nozzle obstruction by islets, and the relatively low production rates [48, 49].

2.2.2 Stirred Emulsification and Internal Gelation

Stirred emulsification and internal gelation involves the production of an alginate-in-oil emulsion in a stirred tank, followed by the addition of an oil-soluble acid [49]. It is a highly scalable alternative to the low productivity extrusion-based cell encapsulation process and can accommodate a much wider range of alginate viscosities. Alginate beads can be obtained from very concentrated (e.g. 5% to 10% alginate) and viscous solutions (up to 100 Pa·s viscosity), which reduces the permeability of the beads towards antibodies [14]. Additionally, stirred mixers are more readily available than nozzle-based encapsulators [49]. The setup of the stirred-tank reactor for alginate bead generation is depicted in Figure 5.

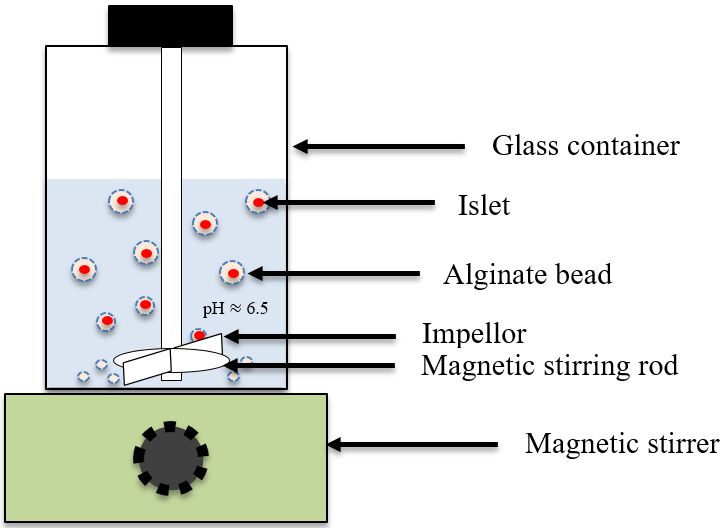

Figure 5. Stirred emulsification and internal gelation setup for microbead generation. Alginate microdroplets are produced in a continuous organic phase via impellor agitation. The droplets then undergo internal gelation upon addition of acetic acid.

Stirred emulsification processes employ the internal gelation technique for alginate gel formation, rather than the commonly used external gelation technique in nozzle-based encapsulation [50]. Compared to external gelation, alginate bead production using emulsification and internal gelation has the potential for larger scale bead generation [51]. In internal gelation, an insoluble calcium salt, such as $CaCO_3$, is added to the alginate mixture prior to emulsification [52]. The addition of an oil-soluble acid, such as acetic acid, decreases the pH of the aqueous phase, resulting in the liberation of Ca^{2+} ions (Equation 1) that physically cross-link the alginate [52, 53].

$$2H^+ + CaCO_3 \rightarrow H_2CO_3 + Ca^{2+} \quad (1)$$

Internal gelation produces alginate beads with increased gel homogeneity over those produced by external gelation [26]; however, the bead matrices are typically less strong, less dense, and the pore sizes are larger [26, 53]. The reduced density and increased pore size occur because upon addition of the acid, H^+ competes with Ca^{2+} for interactions with the alginate polymer chains [53]. The alginate bead pore size can be controlled simply by manipulating the amount of acetic acid, which dictates the competition between the H^+ and Ca^{2+} [53]. While higher amounts of acid ensures adequate bead gelation, this can also be detrimental to cell survival. Adequate selection of the buffer added to the aqueous phase and the amount of acid added to the organic phase can

minimize the pH drop (e.g. from 7.5 before acidification to 6.5 after acidification) while still allowing bead gelation [49].

Despite its many benefits, stirred emulsification has a few drawbacks for islet encapsulation. As displayed in Figure 5, the stirred emulsification device generally produces highly polydisperse emulsions with poor droplet size control, resulting in a wide bead size distribution [54]. This occurs because the turbulent flow present in the vessel leads to non-uniform distribution of local energy dissipation rates in the fluid. A more uniform bead size distribution is desirable for transplantation applications: islets in larger beads encounter oxygen diffusion limitations [55], while smaller beads can lead to incomplete islet encapsulation [11].

2.3 Transplantation of Microencapsulated Islets in Animal Models of Type 1 Diabetes

The first use of alginate-based microcapsules in the reversal of diabetes in rats was reported in 1980 by Lim and Sun [56]. Nozzle extrusion and external gelation was used to encapsulate islets in alginate-poly-L-lysine microcapsules. Transplantation of these microbeads in the intra-peritoneal cavity of rats with streptozotocin-induced diabetes resulted in insulin-independence for 14 to 21 days post transplantation [56]. A similar technique was used to encapsulate porcine pancreatic islets in alginate-polylysine-alginate beads in 1996. In this study, the microbeads were transplanted in spontaneously diabetic monkeys resulting in diabetes reversal for 120 to 804 days [57]. One year later, alginate-polylysine microcapsules were used for the transplantation of allogeneic cells into a 38-year old human diabetic patient suffering from insulin-dependent diabetes for 30 years. Significant improvements in the patient's quality of life were seen and insulin independence was achieved for a period of 9 months [58]. However, a study conducted in 2006, which used alginate-poly-L-ornithine-alginate beads, was less successful in reaching insulin independence in human patients, though improved glycemic profiles and decreased exogenous insulin requirements were observed [59].

In 2005, external gelation was used to produce uncoated alginate microcapsules encapsulating islets, which were injected into the abdominal cavity of diabetic rats. Insulin independence was achieved in the mice for a period of 7 months post transplantation [60]. Clinical trials for the transplantation of encapsulated xenogeneic porcine insulin-producing cells were conducted by Living Cell Technologies in New Zealand in 2010 [61]. Uncoated alginate-

encapsulated islets from fetal pigs were injected into type 1 diabetic patients intraperitoneally resulting in reduced insulin requirements and in a few cases insulin independence for a period of 4 months [61, 62]. Therefore, encapsulation of allogeneic and xenogeneic pancreatic islet cells using alginate-based microcapsules has shown to be a promising transplantation treatment option that overcomes the limitations of conventional insulin therapy. However, further testing and improvements must be done to achieve robust and repeatable long-term insulin independence in large animals (> 3 years).

2.4 Microchannel Emulsification

Membrane emulsification attracted great interest in the late 1980s due to its ability to produce quasi-uniform droplet emulsions with highly controlled droplet sizes [63]. In membrane emulsification, a liquid phase passes through membrane pores, forming monodisperse droplets in a continuous immiscible fluid phase. In this case, the continuous phase is flowing along the membrane surface, producing a drag force that drives droplet detachment [64]. Similarly, microchannel emulsification involves the production of highly uniform droplets with controlled average sizes through uniform slit-like microgrooves. This attractive technique was developed by Sugiura et al. [65] and requires no external shear stress to be applied, simply involving the spontaneous detachment of dispersed phase droplets in a continuous phase [66]. Common microchannel emulsification types include grooved and straight-through microchannel arrays (Figure 6). Straight-through arrays can handle higher dispersed-phase fluxes (up to 60 L m^{-2} h^{-1}) than grooved arrays [67].

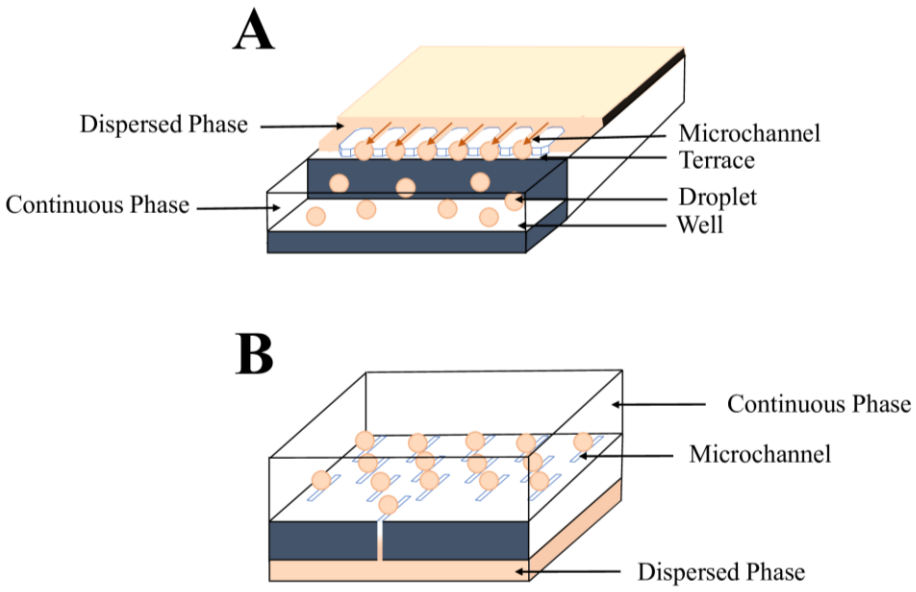

Figure 6. Droplet formation by microchannel emulsification.
A: Grooved microchannel configuration; **B:** Straight-through microchannel configuration.

Several researchers have studied the use of microchannels to produce oil-in-water emulsions [66-69] based on spontaneous interfacial tension-driven droplet generation. The achieved coefficient of variation of droplet size was below 4% [70]. Karen Markwick combined microchannel emulsification technologies with internal gelation to produce solid monodisperse alginate microbeads [16]. However, the beads produced were oversized (~3 mm to 5 mm) and further characterization and optimization of the process was lacking.

2.5 Droplet Formation through a Straight-Through Microchannel

Droplet formation through a straight-through microchannel can be described by a series of steps. Initially, the dispersed phase gradually expands inside the oblong channel, with a discoid shape. The discoid formed then reaches the slot outlet and continues to expand as the fluid exits the channel. A dramatic expansion of the droplet then occurs as the fluid exits the confined oblong channel and enters a spacious volume in the continuous phase. This results in an associated contraction of the dispersed phase inside the channel and a rapid continuous phase flow into the slot towards the contracting dispersed phase, facilitating the formation of a quasi-circular neck in the dispersed phase at the microchannel exit. The neck decreases in diameter until an instantaneous pinch off occurs, producing a dispersed phase droplet [71].

Forces that promote droplet formation include the inertial force associated with the dispersed phase flowing out from the channel, the static pressure difference force, the buoyancy force due to the density difference between the two phases, and the interfacial tension force [72]. The force balance during droplet formation in our microchannel emulsification device is displayed in Figure 7. Unlike in membrane emulsification, the drag force of the continuous phase does not drive droplet formation in microchannel emulsification [64].

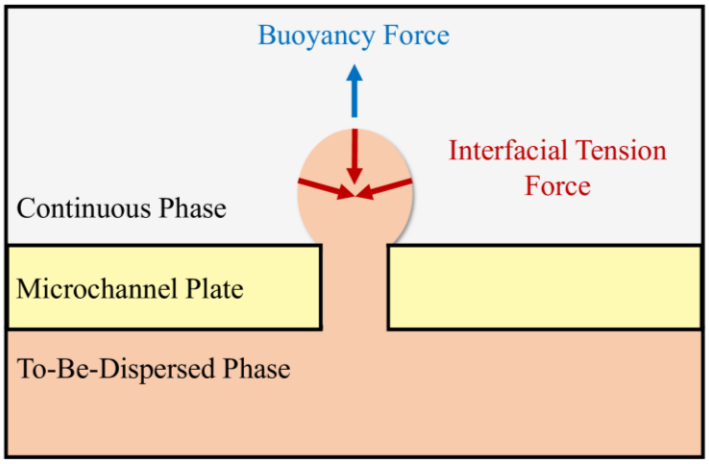

Figure 7. Forces acting in microchannel emulsification droplet formation.
The density of the continuous phase is greater than the density of the dispersed phase.

As shown in Equations 2 to 5 [72, 73], several operating parameters may influence the resulting droplet size, including the cross-flow velocity of the continuous phase, the dispersed phase velocity, the membrane characteristics (microchannel dimensions and wettability), interfacial tension between the dispersed and the continuous phase, as well as the viscosity and the density of the continuous and dispersed phases [74].

$$F_B = \left(\frac{\pi}{6}\right) d_d^3 g \Delta\rho \tag{2}$$

$$F_I = \left(\frac{\pi}{3}\right) d_d^2 U_d \tag{3}$$

$$F_\gamma = \pi d_{hole} \gamma_{ow} \tag{4}$$

$$F_D = 3k_x\pi\eta_c d_d U_c \left[\frac{\left(1+\left(\frac{2}{3}\right)r\right)}{1+r}\right] \quad (5)$$

Where: F_B is the buoyancy force, F_I is the inertial force, F_γ is the interfacial tension force, F_D is the drag force, d_d is the diameter of the droplet, d_{hole} is the hydraulic diameter of the microchannels, g is the acceleration due to gravity, $\Delta\rho$ is the density difference between the two phases, U_d is the dispersed phase velocity through the microchannel, γ_{ow} is the interfacial tension, k_x is a wall correction factor for a sphere (equal to 1.7), r is the ratio of the continuous phase viscosity to the dispersed phase viscosity, U_c is the continuous phase velocity and η_c is the continuous phase viscosity.

The droplet formation depends greatly on the aspect ratio of the microchannel. Continuous outflow of the dispersed phase through the microchannel occurs for aspect ratios lower than a threshold value. For aspect ratios less than ~2.4, increasing the continuous phase velocity flow rate increases the drag force proportionally, which in turn results in the formation of smaller droplets [75]. At higher aspect ratios, a different droplet generation process occurs, whereby the droplet size is virtually independent of the continuous phase velocity [75]. In this case, droplet generation is spontaneously driven by the Laplace pressure difference between the dispersed phase exiting the channel and the dispersed phase inside the channel near the outlet. Rapid shrinkage and cut-off of the droplet neck occurs with higher aspect ratios, forming monodisperse emulsions of small droplets [69].

Dimensionless numbers such as the capillary number and the Weber number are useful in understanding the effects of inertial and viscous forces on the droplet formation, including the capillary number and the Weber number. The capillary number of the dispersed phase represents the relative magnitude of the viscous and interfacial tension forces that are acting during droplet formation, as represented by Equation 6 [76].

$$Ca_d = \frac{\eta_d U}{\gamma} \quad (6)$$

Where: Ca_d is the dispersed phase capillary number, η_d is the dispersed phase viscosity, U is the velocity of the dispersed phase through the microchannel, and γ is the equilibrium interfacial tension between the dispersed and continuous phases.

Below a critical value of the capillary number is the size-stable zone. Uniform droplets are formed with diameters that are independent of the dispersed phase flux. Above the critical capillary number is the continuous outflow zone, where droplet detachment is no longer spontaneous, resulting in very large and nonuniform droplets, or even continuous outflow of the dispersed phase (jetting) [67].

The Weber number (We) is another useful dimensionless number in determining the maximum achievable droplet diameter in an emulsification system. As described in Equation 7, the Weber number is equal to the ratio of a fluid's inertial force to the interfacial tension force, for a given length (droplet diameter) [77].

$$We = \frac{\rho v^2 l}{\gamma} \tag{7}$$

Where: ρ is the density of dispersed fluid, v is the dispersed phase velocity, l is the characteristic length (typically droplet diameter), γ is the interfacial tension.

The droplet diameter can be estimated from the droplet volume by Equation 8 [78].

$$d_{eq} = \left(\frac{6V}{\pi}\right)^{\frac{1}{3}} \tag{8}$$

Where: d_{eq} is the equivalent droplet diameter, and V is the droplet volume.

2.6 Contact Angle and Surface Free Energy

The contact angle, measured by a goniometer, is defined as the angle between a liquid contacting a surface and the plane surface itself. The accuracy of contact angle measurements is diminished by various factors including surface roughness, surface rigidity (Young's modulus), surface homogeneity, temperature, droplet size, humidity and surface impurities [79]. The contact angle provides valuable information related to wettability of fluids on the various microchannel plate surfaces being compared [80]. Solvents of varying hydrophobicity, such as water, octanol, and toluene, can be used to fully understand the hydrophobicity of a material based on the contact angles, which gives an idea of the surface wettability. Wetting is favored by low interfacial free energy, low liquid surface free energy and high solid surface free energy [81, 82].

The surface free energy (measured in mJ/m^2) is a measure of a material's adhesive properties. It is a thermodynamic quantity that describes the state of equilibrium of atoms at the surface of materials [79]. Young's equation (Equation 9) relates the contact angle, θ, to the free energy of the solid surface in a vacuum, γ_S, the solid-liquid interfacial free energy, γ_{SL}, and the liquid surface tension or surface free energy, γ_L [79].

$$\gamma_S = \gamma_{SL} + \gamma_L cos\theta \tag{9}$$

The liquid surface free energy (surface tension) can be measured directly using a dynamic tensiometer. However, there is no direct method to determine the solid surface free energy.

A common indirect method for determining solid materials' surface free energy is the Owens-Wendt method along with Young's equation [79]. The Owens-Wendt method is based on the Bethelot hypothesis, which states that molecules of two interacting substances, present in their surface layer, interact equally to the geometric mean of intermolecular interactions that exist within each substance [82]. The Owens-Wendt method assumes that the surface free energy is a result of two major components: the dispersion interactions, and the polar interactions (Equation 10) [83].

$$\gamma_S = \gamma_S^d + \gamma_S^p \tag{10}$$

Where: γ_S^d is the dispersion component of the solid material surface free energy and γ_S^p is the polar component of the solid material surface free energy. Note that the subscript can be S for solid surfaces (as shown in the equation), L for liquids or SL for solid-liquid interfacial free energy.

Model measuring liquids (water and toluene) with known surface free energy parameters are used in this method. Table 1 summarizes the surface free energy parameters for the two model measuring liquids being used [83, 84].

Table 1. Surface free energy components of model measuring liquids.

[83, 84]

	γ_L (mJ/m^2)	γ_L^d (mJ/m^2)	γ_L^p (mJ/m^2)
Water	72.8	21.8	51.0
Toluene	28.4	26.1	2.3

The surface free energy components of the solid material in question can be calculated from Equations 11 and 12 [79].

$$\sqrt{\gamma_S^d} = \frac{\gamma_t(cos\theta_t + 1) - \sqrt{\left(\frac{\gamma_t^p}{\gamma_w^p}\right)}\gamma_w(cos\theta_w + 1)}{2\left(\sqrt{\gamma_t^d} - \sqrt{\gamma_t^p\left(\frac{\gamma_w^d}{\gamma_w^p}\right)}\right)} \tag{11}$$

$$\sqrt{\gamma_S^p} = \frac{\gamma_w(cos\theta_w + 1) - 2\sqrt{\gamma_s^d\gamma_w^d}}{2\sqrt{\gamma_w^p}} \tag{12}$$

Where: γ_t is the surface free energy of toluene, γ_t^d is the dispersive component of toluene surface energy, γ_t^p is the polar component of toluene surface free energy, γ_w is the surface free energy of water, γ_w^d is the dispersive component of water surface free energy, γ_w^p is the polar component of water surface free energy, θ_w is the contact angle of water and θ_t is the contact angle of toluene.

2.7 Interfacial Tension

To minimize the contact surface energy, the interface of two immiscible fluids tends to form a spherical shape. The size of the spherical droplets depends on the interfacial tension between the two phases. Interfacial tension between two immiscible fluids is a result of the imbalance of intermolecular forces in the two fluids. It represents the work required to increase the contact surface area at the interface. Interfacial tension can be measured using a dynamic tensiometer, which employs the Wilhelmy plate method, the most common method for measuring interfacial tension. A plate made of platinum is used for good wetting upon contact with the liquids being measured. The surface tension, σ, is measured using the Wilhelmy equation (Equation 13).

$$\sigma = \frac{F_{tens}}{L} = \frac{F_g}{L * cos\theta_c} \tag{13}$$

Where: F_{tens} is the tensile force which acts tangentially to the liquid surface, F_g is the gravitational force of the formed lamella on the plate, L is the wetted length (length around the plate that is in contact with the fluid), and θ_c is the contact angle of the fluid on the plate [85].

For iridium-platinum plates, the contact angle can be assumed to be 0^o (complete wetting), simplifying Equation 13. Therefore, to calculate the interfacial tension, the tensiometer must measure the gravitational force of the lamella formed when the plate is found in between the two liquids. However, when the lighter fluid is poured on top of the heavier fluid, there is a buoyancy force that must be taken into consideration.

Initially, the lighter phase is poured into a beaker, and the plate is submerged in this fluid alone. The balance is tared in this state, to compensate for the buoyancy force. Next, the heavy phase replaces the light phase and the plate is completely submerged in this fluid. Finally, the light phase is poured on top of the heavy phase and the plate is pulled back up into the interface between the two phases forming an interfacial lamella. The tensiometer then measures the weight, which represents the gravitational force of the interfacial lamella. This value can then be substituted into Equation 13 to determine the interfacial tension.

2.8 Alginate Bead Characterization

2.8.1 Permeability

Inverse size exclusion chromatography can be used to characterize the permeability of alginate beads [86] by measuring pore characteristics such as volume, surface area and mean size [87]. This technique provides the molecular weight cut-off (MWCO) of a microbead, which is the lowest molecular weight (Da) or size (nm) of a solute in which 90% of the liquid volume inside the pores exclude the solute, as well as the pore size distribution [88]. Unlike other techniques, inverse size exclusion chromatography allows the use of a series of solutes of varying viscous radii and molecular weights, which is useful in further understanding the microcapsule permeability [86].

Inverse size exclusion chromatography is based on the size exclusion principle, which entails that molecules of different sizes will elute (filter) through a stationary phase at different rates [89]. For alginate bead characterization, the beads act as the column packing material (stationary phase), while the mobile phase is a polymer of known molecular weight characteristics [88]. The elution time or elution volume can help determine the molecular weight. The higher the elution time and volume, the lower the molecular weight.

The distribution of a solute between the stationary and mobile phase liquid volumes can be described by the partition coefficient, K_d, described by Equation 14 [88, 90].

$$K_d = c_p/c_i \tag{14}$$

Where: c_p and c_i are the equilibrium solute concentrations in the stationary phase liquid volume and the mobile phase liquid volume, respectively.

K_d can be calculated from the elution volumes measured by inverse size exclusion chromatography using Equation 15 [90]. It represents the fraction of the liquid volume inside the microbead pores accessible to the solutes. The proportion of the pore liquid volume that excludes the solute can be calculated by $1 - K_d$.

$$K_d = \frac{V_e - V_o}{V_t - V_o} \tag{15}$$

Where: V_e is the elution volume of a solute of interest, V_t is the elution volume of a small solute that can fully access the stationary phase pores, and V_o is the elution volume of a solute that is fully excluded from the stationary phase pores (plus the volume of wash buffer acquired prior).

The Stokes radius, R_s, is a measure of the effective radius of the microcapsule pores. This is defined as the radius of a sphere that diffuses at the same rate as the microcapsule that may not necessarily be perfectly spherical. The Stokes radius can be calculated using dynamic light scattering and the Stokes-Einstein Equation 16 [85, 86, 91].

$$D_T = \frac{kT}{6\pi\eta R_s} \tag{16}$$

Where: D_T is the translational diffusion coefficient, k is the Boltzmann's constant, T is the absolute temperature and η is the solvent viscosity.

A study was already conducted using inverse size exclusion chromatography to measure the dimensions of pores and porous volume of 220 µm calcium alginate beads produced via emulsification [89]. The pore volume of the beads were determined to be between 1.92 mL/g and 2.47 mL/g, while the maximum pore radius was found to be between 2.8 nm and 4.0 nm [89]. The pore dimensions of ~1.2 mm beads produced via dripping and external gelation were found to be

between 11 nm and 20 nm [89]. The beads produced via emulsification had a slightly higher pore size normalized to bead diameter compared to those produced by dripping. Another study also showed smaller pores for ~700 µm 1.5% alginate beads produced via extrusion and external gelation compared to beads of the same size and concentration produced by emulsification and internal gelation [14]. Therefore, the gelation method influences the permeability of the alginate beads.

Another study also used inverse size exclusion chromatography to determine the pore characteristics of alginate-poly(L-lysine)-alginate (APA) microcapsules produced via extrusion and external gelation with protein standards and polydisperse dextran [92]. Using a 0.5% alginate concentration, the largest pore diameter was determined to be between 7.8 nm and 8.0 nm in diameter, while the 1.0% alginate beads had slightly lower pore diameters between 7.2 nm and 7.4 nm, as expected [92]. This study demonstrated that the bead pore diameters depend on alginate concentration as well as alginate formulation.

Characterizing the permeability of alginate beads for islet encapsulation is useful to predict the diffusion behaviour of insulin, nutrients, oxygen, antibodies, and immune cells across the porous alginate microcapsules. To avoid the diffusion of antibodies and access to islets by the host immune system, the exclusion limit of the porous membrane is typically set to the size of IgG class antibodies (approximately 5.2 nm viscosity radius), which are the smallest antibodies [86].

2.8.2 Mechanical Strength

The mechanical stability of the alginate beads is an essential characteristic that determines the success or failure of the encapsulation material *in vivo*. The capsules should show enough strength to be able to withstand any shear forces that may occur during the implantation process [93]. Furthermore, the beads should be able to endure abrupt changes in microenvironment. There exist several factors that affect the mechanical stability of the alginate beads including alginate viscosity, alginate concentration, resultant bead size, alginate type, gelling cation type, gelling time, storage solution, cell load, and gelation temperature [94, 95]. Depending on these factors, the compression modulus and shear modulus of alginate hydrogels typically range from 1 to >1000 kPa, and 0.02 to 40 kPa, respectively. For example, alginate with a higher G content is expected to interact more strongly with divalent cation solutions, and therefore should form microcapsules

with higher compression and shear moduli than alginate with higher M content [93]. Increasing gelation time increases the bead strength up to a certain saturation point after which the strength is expected to decrease. The uronic acid molecules in alginate form junction zones within the gel in the cross-linking process, and eventually with time, the number of junction zones will reach saturation. For longer gelation times, there is increased susceptibility for uncoupling in the existing junction zones [94].

To measure the mechanical stability of the resultant microbeads, compression tests can be performed. A common instrument for compression testing is a Texture Analyzer, useful in determining the strength and elasticity of gels, pharmaceuticals, and food products [94]. The force and time required to compress individual microcapsules to 60% deformation can translate to the strength and elasticity of the beads, respectively [94]. In this technique, individual beads are placed on a plate, and the machine probe is moved towards the bead at a speed of 0.5 mm/s, with a trigger force set to 2 g. The force (in grams) is quantified at a 60% compression of the beads [94].

2.8.3 Composition

Spectroscopy instruments, including UV-Vis spectrophotometers, Infrared spectrometers, mass spectrometers and Raman spectrometers, share the common purpose of measuring the chemical composition of a product based on the interaction between electromagnetic radiation and the compounds present in the sample. Raman spectroscopy is an attractive characterization technique as it provides both qualitative and quantitative data on the product in question [96]. This technique involves the excitation of molecules with an incident light, followed by the reflection of this light at a wavelength that depends on the molecules present. The frequency and intensity of scattered radiations are measured by the Raman spectrometer.

Raman spectrometry is based on the Raman effect, which entails the inelastic scattering of a fraction of the photons from a molecule, causing them to have a different energy from that of the incident photon. As a result, when a sample is illuminated by a monochromic laser beam in a Raman spectrometer, a scattered light is produced, with a different (usually lower) frequency than the incident light, depending on the molecules present in the material. The resultant intensity vs. wavelength graph is named the Raman spectrum, which can be used to determine the chemical composition of the product [97]. Samples are usually dissolved in water prior to analysis because

the Raman scattering by water is typically low [96]. Raman spectrometer laser sources include Argon ion (488 nm and 514.5 nm), Krypton ion (530.9 nm and 647.1 nm) and Near Infrared (IR) diode (785 nm and 730 nm) lasers. The advantage of using a longer wavelength laser source, such as the Near IR diode laser, is that a higher power can be obtained without sample photodecomposition or fluorescence [98].

Confocal Raman microscopy is a non-invasive and label-free approach to detect local concentrations of alginate throughout the gel volume and track structural changes after *in vivo* transplantation [99].

2.9 Microencapsulated Cell Enumeration and Survival

2.9.1 Beta Cell Lines

The efficacy of beta cell lines in type 1 diabetes research depends, among other criteria, on their responsiveness to glucose compared to that of normal beta cells in isolated islets. Commonly used insulin-secreting beta cell lines include rat insulinoma cell line (RIN), hamster pancreatic beta cells (HIT), transgenic mouse insulinoma cell line (MIN), insulinoma cell line (INS-1), and beta-tumour cells (βTC) [100]. These cell lines originate from insulinoma in hamsters (HIT), mice (MIN, βTC) and rats (RIN, INS-1) [101].

The cell lines that demonstrate good insulin secretion in response to elevated glucose concentrations include INS-1E, MIN6, and HIT-T15. However, the insulin content in HIT-T15 and βTC cells is lower than that in normal beta cells [102, 103]. INS-1E cells are stable over 116 passages; however, they require toxic mercaptoethanol in their culture media [104], similar to MIN6 cells. An attractive feature of MIN6 cells is their ability to form islet-like clusters [105].

2.9.2 Cell Enumeration and Viability Assessment

Two commonly used cell quantification methods are cell enumeration using a hemocytometer and packed cell volume measurements. Cell enumeration using a hemocytometer can be combined with trypan blue staining, which colours cells with compromised membranes. [106]. Similarly, cells can be enumerated using automated particle counters for example using flow cytometry. Here, DNA-binding dyes such as propidium iodide can be added to identify dead cells based on dye permeability [107]. A drawback to these manual or automated cell enumeration

techniques is the difficulty in accurately quantifying cells in aggregates. Packed cell volume (PCV) is another technique to measure cell volume and monitor cell growth. It involves the use of a PCV tube in which a small sample of the cells suspended in medium is centrifuged, forming a pellet at the bottom of the tube. The volume of the pellet can then be easily read from the PCV tube. This technique is quick and easy and can be considered more accurate as it does not require manual cell counting, which is may result in human error. However, the main drawback of this technique is that it does not distinguish between viable and non-viable cells.

PCV, hemocytometry and flow cytometry require degelling of the microbeads to release cells prior to enumeration. This extra processing step may lead to death or loss of cells. A technique that enables qualitative assessment of cell number and viability in microbeads is live/dead staining, for example using calcein AM and ethidium homodimer-1 dyes. In living cells, calcein AM is hydrolysed into calcein, causing cells to become fluorescent green. Similar to trypan blue or propidium iodide, ethidium homodimer can only enter dead cells through their compromised membrane, staining the nucleic acid into a fluorescent red. The stained cells can then be imaged under epifluorescence illumination to determine the number of live and dead cells [81].

In summary, the technology of microchannel emulsification may be a scalable approach to encapsulate cells in uniform alginate microbeads. Continued development and optimization of the microchannel emulsification device will involve considerations of interfacial tension, density, viscosity, surface free energy, and the critical capillary number. The microbeads generated can be characterized mechanically using texture analysis and physically using inverse size exclusion chromatography and confocal Raman spectroscopy. There also exist quantitative (flow cytometry, hemocytometry) and qualitative (fluorescence microscopy) techniques for assessing the viability of encapsulated cells. The following sections describe the optimization and characterization of the microchannel emulsification device that were conducted in this project.

3 Thesis Objectives

To alleviate the drawbacks with current encapsulation devices, including difficulties in microbead size control and incomplete immunoprotection, a novel microchannel emulsification prototype was previously designed by Karen Markwick [16]. However, the device lacked control in the size of beads achieved and was not yet tested for encapsulated cell viability or bead mechanical properties. Overall, the goal of this project was to optimize and characterize the microchannel emulsification device to ensure the production of durable, ~600 μm alginate microbeads with a coefficient of variation <10% at production rates exceeding 100 mL/h. The device should be able to use alginate viscosities up to ~3 Pa·s similar to previously transplanted emulsion-generated beads [14, 15] and the process should maintain cell viability. We hypothesized that this bead size and alginate viscosity would prevent the diffusion of antibodies and immune cells towards islets, while maintaining sufficient oxygenation and viability of microencapsulated islets [13].

The project was separated into three main aims: (1) Optimization and characterization of the current bead production process via microchannel emulsification to achieve the target bead size and uniformity; (2) durability, permeability and concentration profile measurements of the beads produced using our microchannel emulsification device compared to those produced using the previous stirred-tank emulsification process; (3) assessment of the effect of the microchannel emulsification process conditions on the viability of encapsulated mammalian free cells and cell aggregates.

3.1 Optimization and Characterization of Alginate Bead Production via Microchannel Emulsification

The microchannel emulsification setup for the production of alginate microbeads using a heavier continuous phase fluid, developed by Karen Markwick [16], is shown in Figure 8. The device was able to produce beads as small as 3 mm in diameter, with a relatively narrow size distribution of <10% at a production rate of 4 mL/min/channel [16].

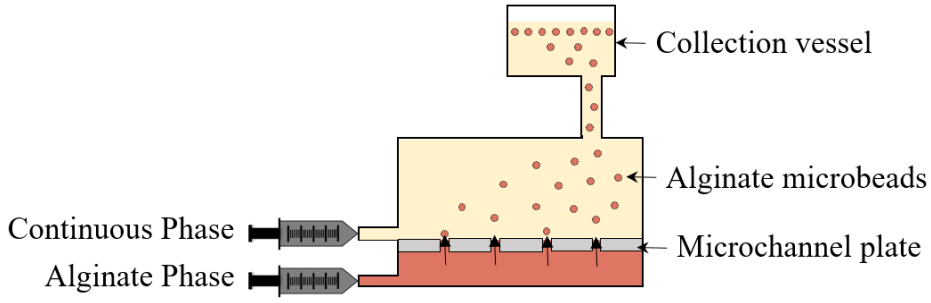

Figure 8. Current microchannel emulsification setup for alginate bead production. Alginate microbeads were produced by continuous microdroplet formation via microchannel emulsification combined with subsequent droplet internal gelation.

In this work, experiments were conducted to determine the optimal process conditions required to produce smaller alginate beads at maximal production rate. The independent variables that were considered were the alginate phase flow rate, alginate concentration, microchannel material (Fluorinated ethylene propylene (FEP), Polytetrafluoroethylene (PTFE), or Frosted Ultra Detail Plastic 3D printed by Shapeways), and continuous fluid (Novec^{TM} 7500 engineered fluid, light mineral oil, or glycerol trioleate). The continuous phase flow rate was not tested because it has little to no impact on alginate bead size and uniformity in microchannel emulsification processes [108].

3.2 Alginate Bead Characterization

The alginate beads produced via microchannel emulsification were assessed in terms of their physico-chemical characteristics. To determine the pore dimensions, as well as the porous volume of microbeads, inverse size exclusion chromatography was conducted in collaboration with the laboratory of Igor Lacík (Slovak Academy of Sciences). In literature, the maximum pore size of 1.5% alginate beads was found to be 5.8 nm, measured using atomic force microscopy (AFM) [109]. It was expected that higher alginate concentrations will lead to smaller pores, while lower alginate concentrations will result in bigger pores.

Alginate bead mechanical strength and elasticity analysis were also conducted by the Lacík lab, using a Texture Analyzer XT. In literature, the rupture force of sodium alginate gel (produced via extrusion and external gelation) under uni-axial compressive strain was determined to increase up to a certain gelling time, after which it remained constant at a value of greater than 40 N [110].

A similar trend was expected for alginate beads produced using microchannel emulsification, since after a certain gelation time, all polymer strands are cross-linked, and further gelation does not change the physical structure. The expectation would be that higher alginate concentrations should lead to higher rupture forces, since increased concentration provides more binding sites for Ca^{2+} ions [111].

Alginate bead swelling in various storage solutions was also assessed overtime. The storage solutions that were tested were: 1) PBS (positive control); 2) DMEM + 10% FBS (negative control); 3) HEPES-buffered saline solution + 100 ppm NaN_3; 4) HEPES-buffered saline solution + 2 mM $CaCl_2$; 5) DMEM + 100 ppm NaN_3; 6) DMEM + 2 mM $CaCl_2$ + 100 ppm NaN_3. The presence of NaN_3 in storage medium is useful in preventing sample contamination overtime. The $CaCl_2$ is expected to maintain the structural stability of the alginate beads. The presence of Na^+ ions in a storage medium such as PBS is expected to cause bead swelling, followed by degradation. This occurs because the Na^+ ions undergo ion-exchange with the Ca^{2+} ions that are binding with carboxyl groups and contributing to cross-linking. As a result, the electrostatic repulsion among the carboxyl group increases, resulting in chain relaxation and gel swelling. Then, the Ca^{2+} diffuses out after some time, causing the bead to disintegrate [112]. HEPES-buffered saline solution is used as the solvent in some storage media rather than reverse osmosis (RO) water to ensure a controlled pH, since pH has an impact on bead swelling. Low pH results in less bead swelling since less ionization of carboxylic acid groups occurs [111].

3.3 Microencapsulated Cell Survival Assessment

The survival of MIN6 free cells and aggregates encapsulated using the microchannel emulsification and stirred-tank emulsification procedures was assessed using various techniques including live/dead staining, flow cytometry and hemocytometry. It was expected that longer gelling times (residence time of beads in acetic acid) would result in higher cell death. Thus, the gelling time was optimized to achieve enough alginate bead gelation with minimal cell death. Furthermore, the viability at various steps in the microchannel emulsification encapsulation process was quantified to determine the most likely cause of cell death.

4 Materials & Methods

4.1 Alginate Solution Preparation

The 0.5%, 1.5% and 2.5% alginate solutions were prepared by dissolving alginate (FMC Manugel® GHB alginic acid, FMC BioPolymer, Philadelphia, USA, Lot # G0600201) into HEPES buffered saline solution (10 mM (4-(2-hydroxyethyl)-1-piperazineethanesulfonic acid (HEPES, ThermoFisher Scientific, Waltham, USA), 170 mM sodium chloride (Sigma-Aldrich, Saint-Louis, USA), pH 7.4). Once fully dissolved, the alginate solution was autoclaved for 30 minutes using the liquid cycle.

4.2 Surface Tension Measurements

The surface tensions of the continuous and dispersed phases were measured using a DCAT 9 Dynamic Contact Angle Meter and Tensiometer (Particle and Surface Sciences Dataphysics, Gosford, Australia) that employs the Wilhelmy plate method. The device was used with PT 11 and the standard surface tension test configurations were modified to 1 mg surface detection threshold and 11 mm immersion depth. Using a motor speed of 1 mms^{-1}, the continuous phases tested were light mineral oil, glyceryl trioleate and 3M™ Novec™ 7500 Engineered fluid (3M, London, Canada). Three different concentrations of the dispersed phase were tested (0.5, 1.5 and 2.5% alginate) with a slower motor speed of 0.1 mms^{-1} due to the viscous properties of alginate.

4.3 Viscosity and Density Measurements

Dynamic viscosity measurements of autoclaved alginate solutions at 25°C and 37°C over a shear rate range of 0 to 600 s^{-1} were performed using Anton Paar MCR 302 Rheometer with a double gap configuration. The effect of shear rate on alginate viscosity was fitted to the Cross model [113] in Equation 17:

$$\eta = \eta_\infty + \frac{\eta_0 - \eta_\infty}{1 + (K_c\dot{\gamma})^m} \tag{17}$$

Where: η is the measured apparent viscosity, $\dot{\gamma}$ is the shear rate applied, η_0 is the zero-shear viscosity, η_∞ is the infinite shear viscosity, m is the Cross rate constant and K_c is the Cross time constant.

The effect of alginate concentration on zero-shear viscosity was described by the Huggins Equation 18 [114]:

$$\eta_0 = \eta_{solvent} \cdot ([\eta] \cdot c + K_H \cdot [\eta]^2 \cdot c^2) \quad (18)$$

Where: $\eta_{solvent}$ is the viscosity of solvent, $[\eta]$ is the intrinsic viscosity of the solution, c is the alginate concentration (in %) and K_H is the Huggins constant.

The densities of the to-be-dispersed and the three continuous phase fluids considered (Novec^{TM} 7500, glyceryl trioleate, and light mineral oil) were measured using a 25-mL graduated cylinder and a Mettler AE160 balance.

4.4 Microchannel Plate Materials

The microchannel plate materials considered were polytetrafluoroethylene (PTFE) sheets, fluorinated ethylene propylene (FEP) sheets (McMaster-Carr, Elmhurst, USA), and Frosted Ultra Detail Plastic 3D printed by Shapeways (New York City, USA). The PTFE and FEP microchannels were produced using laser micromilling, and channels were tapered such that the top side of the channel was smaller (~680 µm x 180 µm) than the bottom side (~720 µm x 220 µm). The 3D printed plastic plates were printed using UV-cured acrylic polymers: Frosted Ultra Detailed Plastic.

4.5 Contact Angle Measurements

Contact angles between various solvents (water, 1-octanol, and toluene) and the three microchannel plates considered (PTFE, FEP and 3D printed plastic) were determined using an OCA 150 system goniometer (DataPhysics instruments GmbH, Filderstadt, Germany). The test plates were initially sonicated in deionized (DI) water for 30 minutes, and air dried for 24-h. The goniometer used a Hamilton syringe (Sigma-Aldrich, Saint-Louis, USA) to place a static droplet (max 30 µL) of solvent on the plate, and an image of the droplet on the solid surface was immediately captured using SCA-20 software. The software was then used to measure the angle between the liquid-solid and liquid-vapour interfaces. The dosing rates and volumes used for each solvent are summarized in Table 2.

Table 2. Dosing rates and volumes used for water, 1-octanol and toluene for goniometer contact angle measurements.

Solvent	Dosing Rate (µL/s)	Volume (µL)
Water	0.5 (Slow)	5.0
1-octanol	2.0 (Fast)	2.5
Toluene	2.0 (Fast)	2.5

The solid surface free energies of the microchannel plates were calculated indirectly using Young's equation and the Owens-Wendt method (Equations 9 to 12). The liquid surface free energy (surface tension) was measured directly using a dynamic tensiometer.

4.6 Microencapsulation by Microchannel Emulsification

The microchannel emulsification process was based on direct droplet formation and internal gelation. The device was composed of two flow chambers placed above and below a microchannel plate consisting of one to three rectangular straight-through microchannels in parallel.

The to-be-dispersed phase flowing in the bottom chamber consisted of 29.7 mL autoclaved alginate solution, 2.3 mL complete Dulbecco's Modified Eagle medium (DMEM supplemented with 10% fetal bovine serum (FBS), 1% penicillin/streptomycin, 2 mM L-glutamine (all from Thermo Fisher Scientific, Waltham, USA), and 5 mM beta mercaptoethanol (Sigma-Aldrich, Saint-Louis, USA)), 1.65 mL of $CaCO_3$ solution (1 g in 20 mL HEPES buffered saline solution), and 1 mL FBS. For MIN6 cell encapsulation runs, MIN6 cells or aggregates were suspended in the complete DMEM at a concentration of ~13 million free MIN6 cells per mL of complete DMEM or ~450 MIN6 aggregates per mL. The to-be-dispersed phase was introduced into the bottom chamber through inlet tubing attached to a 30 mL syringe (VWR International, Radnor, USA) that was pushed manually or with a Sage Instruments model 355 or model 365 syringe pump (Sage Instruments, Freedom, USA) at flowrates ranging from 0 to 12 mL/min.

The top chamber contained a continuous phase with 0.22 v/v % glacial acetic acid (Thermo Fisher Scientific, Waltham, USA). The continuous phase fluids considered in this study were 3M™ Novec™ 7500, light mineral oil (Thermo Fisher Scientific, Waltham, USA) and glyceryl trioleate (~65%, Sigma-Aldrich, Saint-Louis, USA). An outlet tube, ~10.5 cm in length and 1.3

cm in diameter, was attached to the top of this chamber, leading to a collection vessel (8.0 cm x 12.0 cm x 8.8 cm). The device was designed to achieve control of the continuous phase flow rate using a 60 mL syringe (VWR International, Radnor, USA) and a Harvard Apparatus PHD 2000 Programmable syringe pump; however, the flow rate was kept at zero in this study.

Start-up of the device consisted of initial manual filling of the bottom chamber with the to-be-dispersed alginate phase (~5 mL), followed by the introduction of 200 mL of the acidified continuous through the collection vessel into the top chamber. The alginate syringe pump was then activated at a flow rate of 10 mL/min to purge air bubbles through the microchannels. Next, the flow rate was adjusted back to the desired flow rate to initiate droplet generation. The beads were left in the bath for a given gelling time before separation using a 40 µm nylon cell strainer (Thermo Fisher Scientific, Waltham, USA) and washing (three times in complete DMEM) prior to further analysis. A schematic and photo of this microchannel emulsification process is displayed in Figure 9.

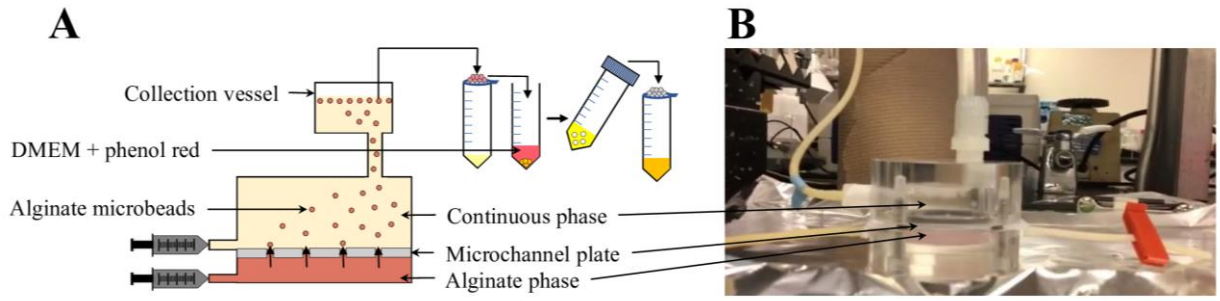

Figure 9. The experimental microchannel emulsification approach for alginate microbead generation.

A: Microbeads were produced via microchannel emulsification and internal gelation followed by rinsing in complete DMEM (three times or until phenol red indicator no longer changes in colour) prior to further product assessment. **B:** Snapshot of the microchannel emulsification device continuously producing 1.5% alginate beads using a PTFE plate with three oblong (~700 x 200 µm) microchannels in parallel.

4.7 Microencapsulation by Stirred Emulsification

The stirred emulsification process was adapted from the process optimized by Hoesli et al. [115]. Initially, 20 mL of light mineral oil was introduced into a spinner flask placed on a magnetic stirrer and agitated at 220 rpm. The alginate phase was prepared by combining 9.9 mL of 1.5%

alginate solution in HEPES buffered saline solution, 550 µL of complete DMEM, and 550 µL 0.05 g/mL $CaCO_3$ solution. This alginate phase was then added slowly to the spinner flask to initiate emulsification. After 12 minutes of agitation, 11 mL of light mineral oil mixed with 0.14 vol% glacial acetic acid was added to the flask to initiate the 8-minute acidification step, and the stir speed was decreased to 200 rpm. 40 mL of HEPES buffered saline solution mixed with 10% complete DMEM was then added to the flask to neutralize the acid. After an additional minute of agitation, the stirrer was turned off, and the oil phase was separated from the beads and aqueous phase using centrifugation at 630 g for 3 min, twice. The beads were then separated from the remaining aqueous solution using a 40 µm nylon cell strainer and washed twice more with complete DMEM.

4.8 Alginate Bead Size Distribution

A sample of the alginate beads produced via the microchannel emulsification process (~ 1 mL) was incubated in 4.5 mL HEPES buffered saline solution, 0.5 mL complete DMEM, and 100 µL of 1 g/L toluidine blue O (Sigma-Aldrich, Saint-Louis, USA), in a 15-mL conical tube (Sarstedt) mounted sideways on a rotary shaker set at 50 rpm agitation for 80 minutes. The stained beads were then dispersed in a 10 cm Petri dish (Thermo Fisher Scientific, Waltham, USA) containing 20 mL of HEPES buffered saline solution combined with 10% complete DMEM. A ruler was placed next to the Petri dish, and a photo was taken using an iPhone 6s 12-megapixel camera (Apple, Canada). CellProfiler [116] was used to determine the mean diameter, surface area moment mean diameter (D_{32}), and volume moment mean diameter (D_{43}).

4.9 Alginate Bead Preparation and Storage for Mechanical Testing

Beads at similar D_{32} values were produced aseptically using both the microchannel and stirred emulsification processes. The beads were then stored in a filtered storage medium consisting of 2 mM $CaCl_2$ and 100 ppm NaN_3 in HEPES buffered saline solution at a 1:10 volumetric ratio and shipped internationally to the Polymer Institute of Slovak Academy of Sciences, Department for Biomaterial Research (Bratislava, Slovakia) for inverse size exclusion chromatography, texture analysis and Raman analysis.

4.10 Compression Testing using a Texture Analyzer

The mechanical strength of the alginate beads was measured using a Texture Analyzer (TA-XT2i, Stable Micro Systems, Godalming, UK) equipped with a mobile probe and software Texture Expert Exceed 2.64. The bursting force was measured up to 95% bead deformation at a compression speed of 0.5 mm/s. The average compression resistance of the alginate microbeads was determined by taking the average bursting force by 70% deformation for a sample of 20 to 30 microbeads.

4.11 Inverse Size Exclusion Chromatography

To measure the molecular weight cut-off (MWCO) of the alginate microbeads, inverse size exclusion chromatography was employed. A 10-mL sample of the microbeads was placed in a 10 x 150 mm glass Omnifit chromatographic column (Omnifit, Cambridge, UK). Pullulan/dextran standards (Polymer Laboratories, American Polymer Standard Corp. and Polysciences) of 3 mg/mL concentration were introduced into the column using a 100 µL loop injector. The mobile phase consisted of HEPES buffered saline solution with 100 ppm NaN_3 and 2 mM $CaCl_2$ (pH 7.4), applied at a flow rate of 0.2 mL/min. The recorded elution volume (V_e) represented the volume at which 50% of the standard was eluted. The void volume (V_o) was determined by the elution volume of a 805,000 Da pullulan standard while the total permeable volume (V_t) was obtained from the elution volume of 62 Da ethylene glycol. From the elution volume, the chromatographic partition coefficient (K_d) was calculated using Equation 15, $K_d = \frac{V_e - V_o}{V_t - V_o}$. The proportion of the pore liquid volume that excluded the pullulan/dextran standards ($1 - K_d$) was plotted against the log of the solute molecular weights to determine the MWCO (the solute molecular weight (Da) in which $1 - K_d = 0.90$). This data was then fitted to the Boltzmann sigmoidal function (Equation 19) [117]. Data acquisition and evaluation was achieved using WinGPC UniChrom (Polymer Standard Service, Mainz, Germany).

$$1 - K_d = k_1 + \frac{k_2}{1 + exp(k_3 - k_4\, log(MW))} \tag{19}$$

Where: MW is the molecular weight of the pullulan/dextran standards and k_i are empirical fitting parameters.

4.12 Raman Spectroscopy

Raman analysis was achieved using a confocal Raman microscope (WITec alpha). The process used a 785 nm laser, an integration time of 8 seconds, and an optical cable of 100 nm. Mathematical processing of the Raman spectra was conducted to remove the background, and to fit sodium alginate to the data. Quantitative analysis was performed as described in Kroneková et al [99].

4.13 MIN6 Cell Culture and Enumeration

MIN6 cells, originally from the laboratory of Dr. Jun-Ichi Miyazaki (Department of Disease-Related Gene Regulation Research (Sandoz), Faculty of Medicine, University of Tokyo, Tokyo, Japan), were obtained from Dr. James Johnson (University of British Columbia, Vancouver) and cultured in complete DMEM. The adherent MIN6 cell culture was maintained using a seeding density of 4×10^4 cells/cm^2 on surface treated T-flasks (Sarstedt), in 20 mL/75 cm^2 complete DMEM. The medium was replaced with warm (37^{o}C) fresh complete DMEM every 2 to 3 days. The cells were passaged at approximately 90% confluency. This was done by removing the medium, rinsing with phosphate-buffered saline solution (PBS), then incubating the cells in 5 mL TrypLE (Thermo Fisher Scientific, Waltham, USA) at room temperature for 5 minutes, after which 10 mL of complete DMEM was added to deactivate the TrypLE. Finally, the resultant solution was centrifuged at 1200 rpm for 5 minutes, then resuspended in complete DMEM. A 100 µL sample of the well-mixed cell suspension was combined with an equal volume of 0.4% trypan blue solution (Sigma-Aldrich, Saint-Louis, USA) for cell counting via hemocytometry.

4.14 MIN6 Cell Aggregate Formation

MIN6 cells were aggregated by adding 5×10^5 cells suspended in 2 mL complete DMEM in each well in an AggreWell^{TM} plate (Aggrewell^{TM} 400, StemCell Technologies, Canada) and incubating for 72 hours at 37^{o}C. The aggregates were then harvested by pipetting with 1-mL cut tips and filtering with 40 µm nylon cell strainer (Thermo Fisher Scientific, Waltham, USA).

4.15 Live/Dead Staining

Cells were stained in a staining solution containing 4 µM calcein AM, 4 µM ethidium homodimer and 8 µM Hoechst (Thermo Fisher Scientific, Waltham, USA) in HEPES buffered saline solution for encapsulated cells, or PBS for free cells. Dead controls were prepared by incubating encapsulated cells in 5 mL of 99% ethanol. Encapsulated cells were incubated in their respective staining solutions for 30 minutes, protected from light, prior to live/dead imaging, while free cells were incubated for 10 minutes. Live/dead imaging was conducted using a fluorescence microscope (IX81, model IX2, Olympus, Tokyo, Japan).

4.16 Bead Degelling and Flow Cytometry

The degelling solution was prepared by adding 55 mM sodium citrate dihydrate (Sigma-Aldrich, Saint-Louis, USA), 10 mM HEPES and 95 mM NaCl to RO water at pH 7.4. Encapsulated cells were added to this degelling solution at a 1:9 volumetric ratio and incubated on a rotary shaker in ice at 90 rpm for 40 to 60 minutes, or until the beads were completely dissolved. The degelling solution was then separated from the encapsulated cells via centrifugation, and the cells were subsequently resuspended in propidium iodide staining solution (12.5 µg/mL in PBS, BD Life Sciences, Mississauga, Canada), incubated at 4^{o}C for 30 minutes, and analyzed using a BD Accuri C6 flow cytometer. Data analysis was then conducted using FlowJo Single Cell Analysis Software v10.

4.17 Statistics

The statistical analysis used for comparing two data samples was a two-tailed t-test, and for comparing multiple data samples, one-way analysis of variance (ANOVA) was applied using JMP statistical software, with $p < 0.05$ considered statistically significant. Following ANOVA analyses where the groups were shown to be significantly different, Tukey and Scheffe post-hoc tests were used to determine which pair of groups were significantly different.

5 Results

In this work, continued improvements and optimization of the microchannel emulsification device led to the generation of uniform alginate beads as low as ~1.5 mm in diameter with coefficients of variation <10% for animal cell encapsulation at throughputs required for clinical islet transplantation (>100 mL/min) [16]. The device was able to use a wide range of alginate viscosities (0.005 to 0.2 Pa·s), useful for achieving islet immunoisolation against immune cells and antibodies. These results were achieved by investigating the effects of various process parameters (e.g. continuous phase density and surface tension, alginate viscosity and flow rate, and microchannel dimensions) on bead size and uniformity. Successful encapsulation of insulin-producing beta cells was also achieved by optimizing the acetic acid concentration in the oil phase as well as the bead residence time in acid. The following sections summarize the results obtained from optimization and characterization experiments conduced for the development of the microchannel emulsification device for beta cell encapsulation purposes.

5.1 Continuous Phase Fluid Assessment

To promote droplet generation in microchannel emulsification, factors that drive droplet detachment (e.g. the density difference between the phases) should be maximized while factors counter-acting droplet detachment (e.g. interfacial tension) should be minimized. Novec^{TM} 7500 was previously identified as a promising continuous phase candidate to generate alginate beads in the microchannel emulsification device based on empirical observations [16]. To quantitatively verify the selection of Novec^{TM} 7500, we compared the density differences and surface tension of various organic phases (including Novec^{TM} 7500), under the assumption that lower surface tensions correlate with lower interfacial tensions.

Although alginate concentration theoretically impacts the fluid surface tension and density, these effects were not found to be significant compared to experimental variability. The average surface tension for alginate solutions of concentrations 0.5% to 2.5% was found to be 0.0551 ± 0.0016 N/m, while the average density was 1020 ± 10 kg/m^3. Figure 10 displays the average density difference measured between the three continuous phase fluids considered and a 1.5% alginate solution, as well as the surface tension of the three organic fluids. Compared to the remaining continuous phase fluids, Novec^{TM} 7500 fluid had the highest density difference with

alginate and the lowest surface tension, both of which favour the formation of smaller alginate droplets. The experimental density difference and surface tension values were similar to the literature expected values of 590 kg/m^3 calculated from the technical data sheet density and 0.0155 N/m [118], respectively. The selection of Novec^{TM} 7500 fluid rather than light mineral oil or glyceryl trioleate can thus be justified by the measurement of surface tension and density difference with the alginate solution. These measurements could be used to select further continuous phase fluids for alginate bead production by microchannel emulsification.

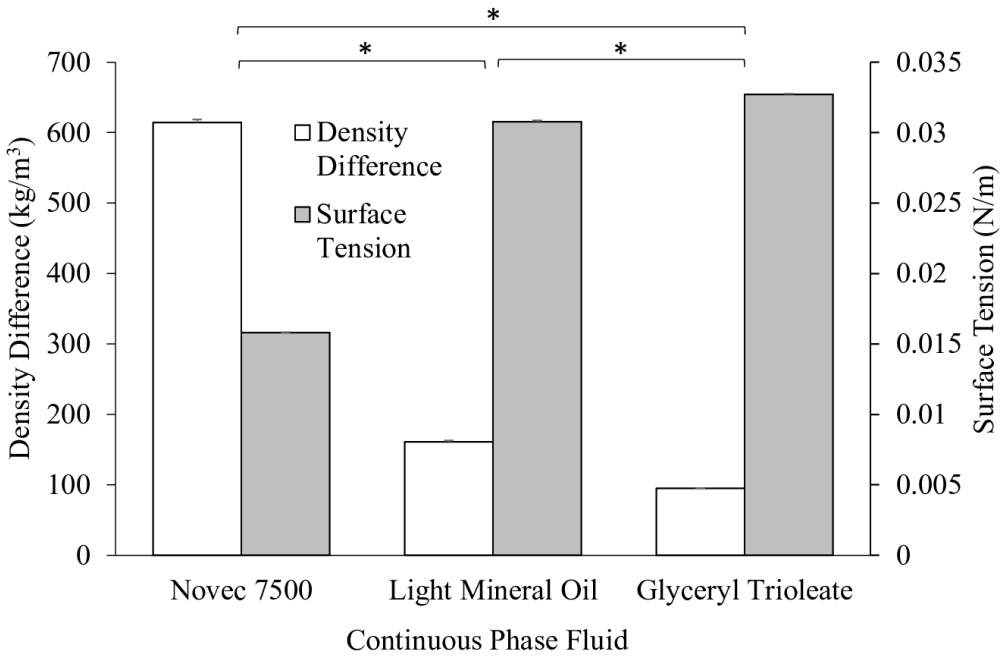

Figure 10. Surface tension of various continuous oil fluids and density difference between these oil phases and a 1.5% alginate phase.

The continuous phase fluids considered in this study were 3M^{TM} Novec^{TM} Engineered Fluid, light mineral oil and glyceryl trioleate. Error bars represent the standard error of n=3 runs, *p<0.05 for both density difference and surface tension.

5.2 Plate Material Selection

Microchannel plate material is another important factor that affects droplet size. In the previous study [16], PTFE was the chosen microchannel plate material for the microchannel emulsification device. To verify this selection quantitatively, surface free energies of various hydrophobic materials were measured and compared. A higher solid surface free energy indicates

enhanced microchannel wetting by the continuous phase fluid, which would promote alginate droplet detachment.

All three materials considered (PTFE, FEP and 3D printed plastic) are hydrophobic, with water contact angles greater than 90°. Table 3 presents the component and total surface free energies of PTFE, FEP, and 3D printed plastic, calculated using the average contact angles (measured using a goniometer), and the Owen-Wendt method (Equations 10 to 12). The contact angle of toluene on a 3D printed plastic surface was reported to be 0°, since complete wetting was observed.

Table 3. Average measured contact angles of water and toluene on various microchannel materials, and the calculated component and total solid surface free energies based on the Owen-Wendt model.

Solid Surface Material	Solvent	Average Contact Angle (°)	$\gamma_S^d \left(\frac{mJ}{m^2}\right)$	$\gamma_S^p \left(\frac{mJ}{m^2}\right)$	$\gamma_S \left(\frac{mJ}{m^2}\right)$
PTFE	Water	106 ± 2	28 ± 1	0.1 ± 0.1	28 ± 1
	Toluene	23 ± 2			
FEP	Water	103 ± 1	21 ± 1	0.8 ± 0.2	22 ± 1
	Toluene	40 ± 1			
3D printed plastic	Water	121 ± 5	36 ± 13	2 ± 14	38 ± 30
	Toluene	0			

The experimentally determined surface free energies of PTFE and FEP were of the same order of magnitude as values reported in the literature (20.0 $\frac{mJ}{m^2}$ [119] and 17.9 $\frac{mJ}{m^2}$ [120], respectively). As expected, the surface free energy of PTFE was higher than FEP, suggesting that PTFE would enable enhanced wetting of the continuous phase fluid in the microchannel emulsification process [82]. For this reason, we continued using PTFE as the microchannel plate material for further microchannel emulsification experiments.

5.3 Process Optimization and Characterization

5.3.1 Characterization of Alginate Viscosity

To quantify the viscous forces present in the dispersed phase of the microchannel emulsification device, the dynamic viscosity of alginate solutions at various concentrations were measured. Alginate is a shear-thinning fluid. As expected, the dynamic viscosity decreased upon increasing the shear rate applied (Figure 11A). This experimental data was fitted to the Cross model (Equation 17) using Matlab to obtain the zero-shear viscosity of alginate at the concentrations and temperatures considered, as summarized in Figure 11B and Table 4. The exponential increase in zero-shear viscosity as a function of alginate concentration was fitted to the Huggins equation (Equation 18) to obtain the intrinsic viscosity at 25^{o}C (13.98 Pa·s) and 37^{o}C (11.58 Pa·s), using a Huggins coefficient of 0.5. As expected, the intrinsic viscosity varied inversely proportionally with temperature, following the behavior described by the Arrhenius equation [121]. The intrinsic viscosities obtained fall within the expected range of 4.2 to 30 Pa·s for alginate [122]. With these intrinsic viscosities, the zero-shear alginate viscosity at any alginate concentration can be calculated using the Huggins equation (Equation 18).

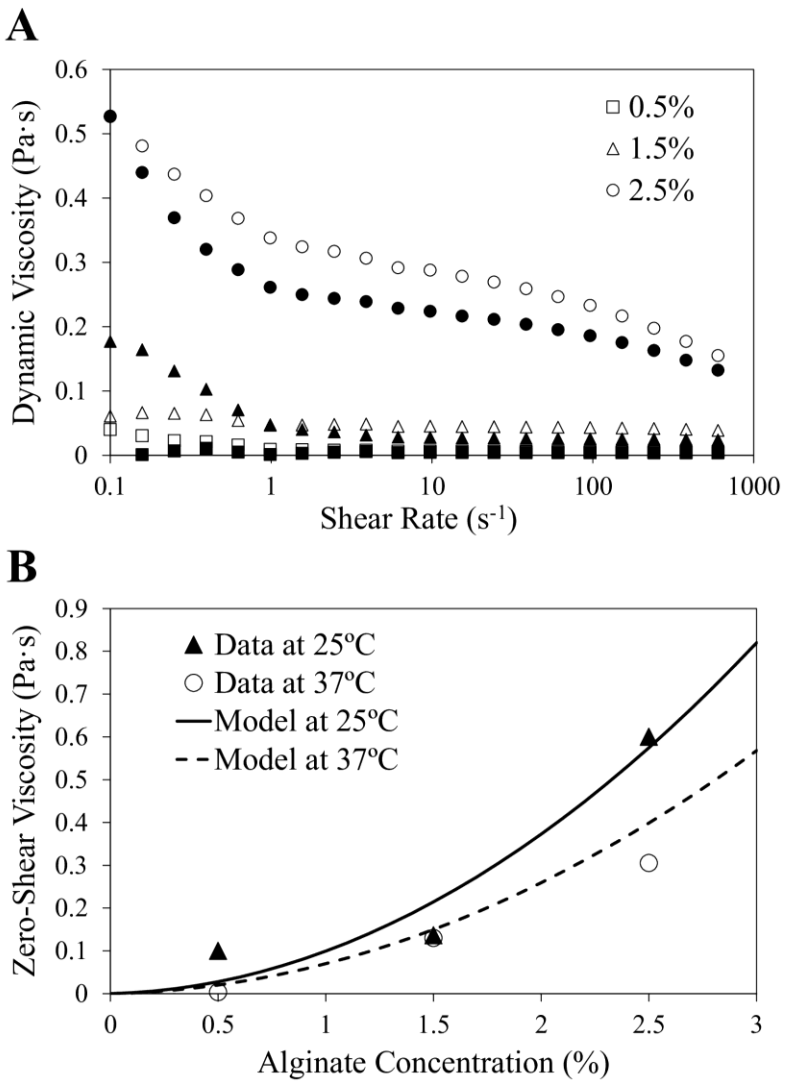

Figure 11. Alginate viscosity as a function of shear rate and alginate concentration. **A:** Dynamic viscosity of alginate at various at shear rates between 0 and 600 s^{-1} measured using a rheometer shared by the labs of Prof. Richard Leask and Prof. Milan Maric at McGill University. Filled and hollow data points represent runs conducted at 25ºC and 37ºC, respectively. **B:** Relationship between the zero-shear viscosity and concentration of alginate solution at 25ºC and 37ºC. The data was fitted to the Huggins model (R^2 of 0.944 at 25ºC and R^2 of 0.994 at 37ºC). These graphs were generated with the help of Chloé Selerier (undergraduate student, McGill University).

Table 4. Cross model parameters[a] for the alginate solution concentrations (c) used in this study at a system temperature of 25°C[b].

c (%)	η_0 (Pa·s)	η_∞ (Pa·s)	K_c (s)	m
0.5	0.10	0.01	20.31	0.84
1.5	0.14	0.04	117.80	0.38
2.5	0.60	0.18	1.45	0.46

[a] The Cross model equation is $\eta = \eta_\infty + \frac{\eta_0 - \eta_\infty}{1 + (K_c\dot{\gamma})^m}$, where η is the measured apparent viscosity, $\dot{\gamma}$ is the shear rate applied, η_0 is the zero-shear viscosity, η_∞ is the infinite shear viscosity, m is the Cross rate constant and K_c is the Cross time constant [107].

[b] 25°C was the system temperature used in all microchannel emulsification experiments in this study.

To estimate the alginate viscosity flowing inside the microchannels of the microchannel emulsification device for a given alginate concentration, a shear rate of 420 s^{-1} was substituted in the Cross model, along with the parameters found in Table 4. The shear rate in the microchannels of 420 s^{-1} was calculated by dividing the fluid velocity through the channel by the hydraulic radius of the channel (details in Appendix 10.3). With these model parameters, it is possible to estimate the dynamic viscosity of any alginate solution in the microchannel emulsification device.

5.3.2 Effect of Flow Rate and Viscosity on Flow Regime and Bead Diameter

Alginate bead size control in the microchannel emulsification device can be achieved with knowledge of the critical capillary number of the system as well as assessment of the influence of alginate viscosity and flow rate on bead diameter. Figure 12A summarizes the average flow rate that resulted in a first transition (elongated droplet formation with a neck) and jetting (continuous outflow of the dispersed phase through the microchannel) for alginate phases of increasing viscosity. Increasing the alginate viscosity resulted in a decrease in the alginate flow rate (or velocity) required to reach first transition and jetting (Figure 12A), as expected based on the capillary number relation (Equation 6).

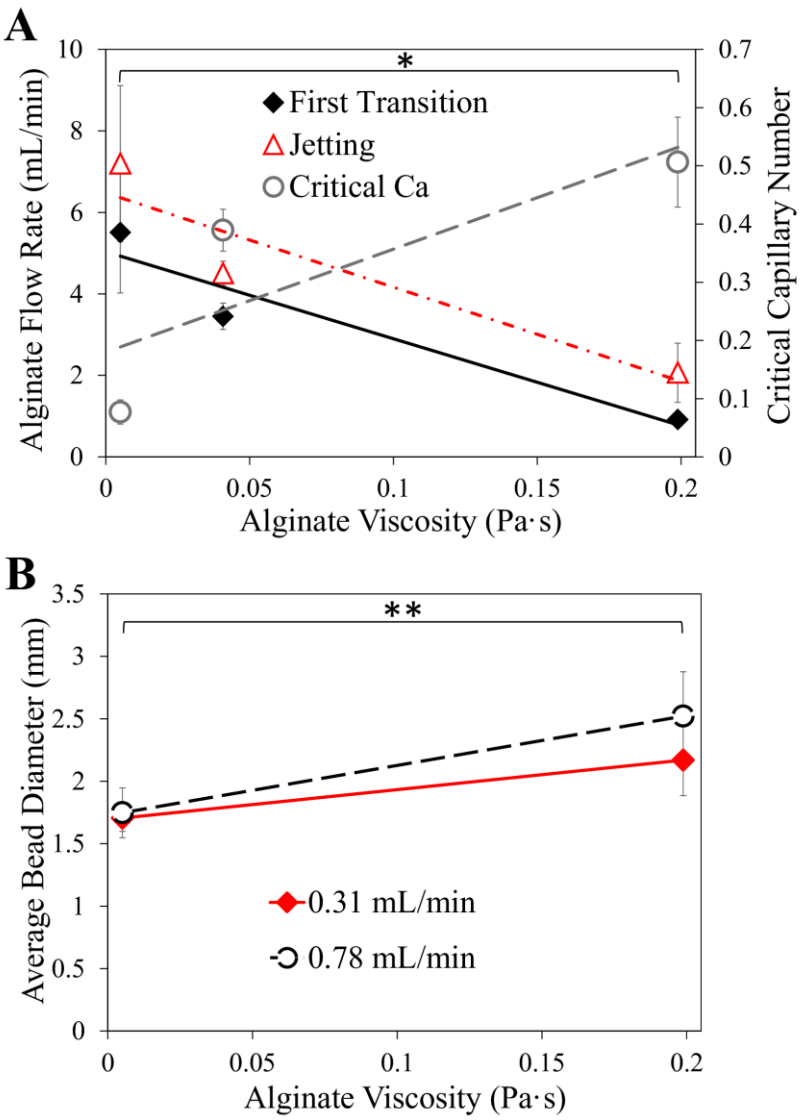

Figure 12. Characterization of the alginate flow regime through microchannels and the average microbead diameter as a function of alginate viscosity and flow rate.

A: Alginate flow rate resulting in first transition (droplet elongation with a neck) and jetting (continuous outflow of the dispersed phase through the microchannel) at a system temperature 25ºC as a function of alginate viscosity. The critical capillary number was calculated from the first transition flow rate. Error bars represent standard error of n=3 runs, *p<0.05 (first transition only). **B:** Effect of alginate viscosity and flow rate on average bead diameter. Full factorial experimental data is found in the supplementary Table 7 (Appendix 10.2). Error bars represent standard error of n=2 runs, **p<0.01.

A preliminary approximation of the system critical capillary number was conducted to characterize the flow rate at which jetting would occur in our microchannel emulsification system. The critical capillary numbers for the alginate solutions considered, summarized in Table 5 and Figure 12A, were calculated using the flow rates at first transition and the viscosity data in the previous section. Since the interfacial tension between alginate and Novec^{TM} 7500 was not measured in this study, an approximation of 43 mN/m was used based on the interfacial tension between similar organic compounds (Novec^{TM} 7300 and 7700) and water from literature [123]. This study enabled a preliminary understanding of the range of alginate flow rates that result in uniform spontaneous droplet generation (rather than unstable jetting), necessary for further characterization of the microchannel emulsification device.

Table 5. Alginate fluid properties used in the calculation of the critical capillary numbers for each alginate concentration in this flow system at T=25°C.[a]

Alginate Concentration (%)	Alginate Viscosity (Pa·s)	First Transition Flow Rate (mL/min per channel)	Average Fluid Velocity in the Channel (m/s)	Critical Capillary Number
0.5	0.0051	5.5 ± 1.5	0.66 ± 0.18	0.08 ± 0.02
1.5	0.041	3.5 ± 0.3	0.41 ± 0.04	0.39 ± 0.04
2.5	0.20	0.9 ± 0.1	0.11 ± 0.02	0.51 ± 0.08

[a] The interfacial tension value used for the critical capillary number calculation was obtained from literature for a similar Novec/water system: 43 mN/m [123].

A 2^2 full factorial design of experiments with three center points and two replicates was then conducted to assess the significance of the effects of alginate viscosity, alginate flow rate, and the interaction of the two, on the average diameter of alginate beads formed using the microchannel emulsification process. The low level flow rate was chosen to be the minimum flow rate required to achieve droplet formation using all alginate solutions, while the high level was the maximum flow rate that generates droplets without jetting. Figure 12B shows that increasing the alginate viscosity from 0.01 Pa·s to 0.20 Pa·s resulted in a significant increase in the average bead diameter. In contrast, the effect of the alginate flow rate on the average bead diameter was found to be insignificant over the range of 0.31 mL/min to 0.78 mL/min. From these results, the bead

production rate can be modified by changing the alginate flow rate without affecting the bead diameter; however, tuning the alginate viscosity would alter the bead size. On the other hand, neither factor significantly impacted bead uniformity when operating below the critical capillary number. The detailed full factorial experimental data is found in Table 7 located in Appendix 10.2 Supplementary Tables.

5.3.3 Alginate Bead Size Distribution

To determine whether the microchannel emulsification system leads to the expected increase in bead uniformity compared to the existing stirred emulsification process, the bead size distributions were measured for both processes. Figure 13A displays proof-of-concept alginate beads produced using the microchannel emulsification device with a PTFE microchannel plate (700 µm x 200 µm channel dimensions), Novec^{TM} 7500 continuous phase fluid, 1.5% alginate concentration, 0.55 mL/min alginate flow rate and an 8-minute gelation time. These beads were highly uniform in size (coefficient of variation < 10%) when compared to the beads produced using the stirred emulsification device (Figure 13C; coefficient of variation > 60%). The microchannel emulsification bead size distribution (Figure 13B) displayed a normal distribution centered around 2210 µm bead diameter with a full width at half maximum (fwhm) of 440 µm (20%). The stirred emulsification impeller rotation speed was adjusted to obtain a similar average bead diameter as observed during microchannel emulsification, according to previously described procedures [115]. The size distribution of the beads produced via stirred emulsification (Figure 13D) displayed a slightly skewed distribution centered around a similar diameter (2190 µm) as in microchannel emulsification, but with a much larger fwhm of ~1200 µm (55%). This large size distribution was also found in literature for the same stirred emulsification process (56 ± 8% standard deviation) [49]. Evidently, microchannel emulsification is a more controlled process that can generate uniform alginate beads relative to stirred emulsification.

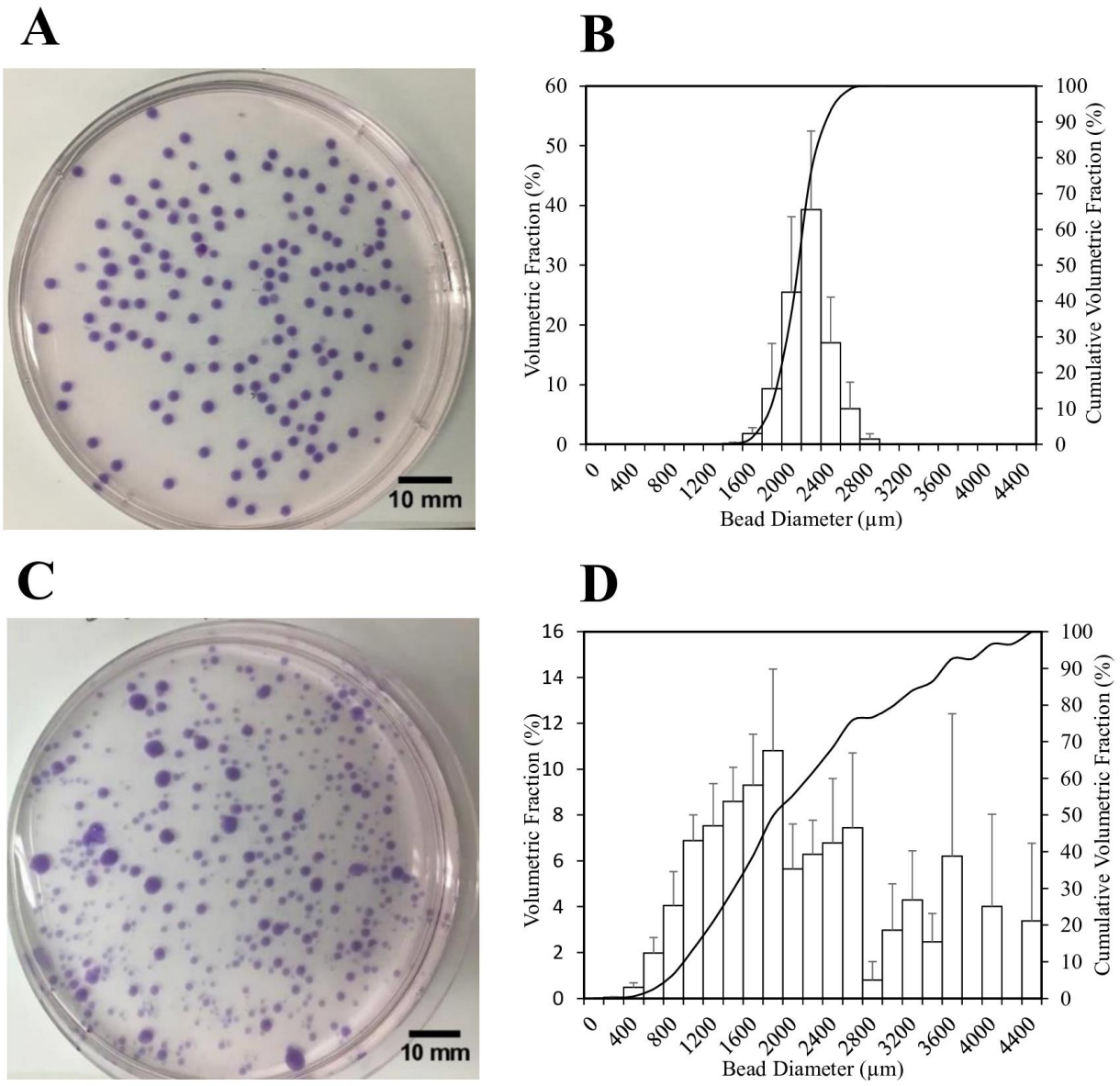

Figure 13. Proof-of-concept alginate beads generated via microchannel and stirred emulsification processes and the resultant bead size distributions.

A: Image of 1.5% alginate bead sample produced via microchannel emulsification; **B:** Size-distribution of 1.5% alginate beads produced using microchannel emulsification; overall average bead diameter is 2210 µm with fwhm = 440 µm (20%); **C:** Image of 1.5% alginate bead sample produced via stirred emulsification; **D:** Size-distribution of 1.5% alginate beads produced via stirred emulsification; overall average bead diameter is 2190 µm with fwhm = 1200 µm (55%). Error bars represent standard error of n=3 runs.

5.4 Mechanical Properties

5.4.1 Effect of Storage Medium on Bead Swelling

Several bead characterization methods, such as the mechanical and physical tests conducted in this study, cannot be conducted immediately after bead production. Bead samples risk contamination, swelling and degradation, which would alter the mechanical and physical properties of interest during the time between production and characterization. As such, a storage medium that preserves bead mechanical integrity and permeability over time was desired. Adding NaN_3 to the storage medium was essential for long-term contamination prevention of the alginate microbead samples. Still, bead storage in HEPES buffered saline solution with 100 ppm NaN_3 resulted in bead degradation after only 48 hours of storage, as shown in Figure 14, suggesting that the concentration of $CaCl_2$ in the buffer solution was inadequate to maintain mechanical stability.

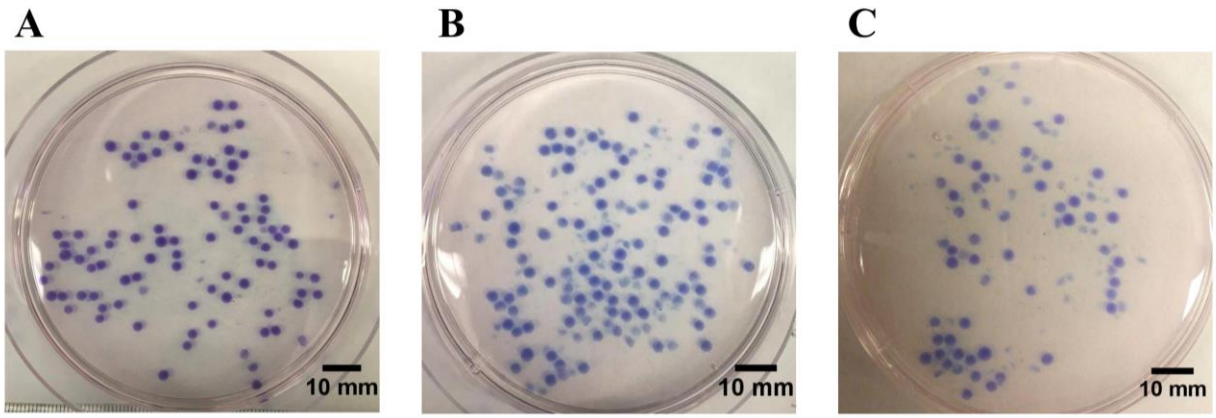

Figure 14. Observed bead degradation of 1.5% alginate beads stored in HEPES + 100 ppm NaN_3 for up to 48 hours.
A: Initial; **B:** 24 hours; **C:** 48 hours.

A similar result was obtained for beads stored in phosphate-buffered saline (PBS), as expected from the presence of phosphate acting as chelator. On the other hand, adding 2 mM $CaCl_2$ resulted in no apparent bead swelling or degradation over 48 hours. This result implies that $CaCl_2$ is a useful ingredient to maintain mechanical stability in a storage medium over time.

To determine whether $CaCl_2$ also maintained the mechanical stability of alginate beads over a longer period (one month), the effect of alginate bead storage in complete DMEM on bead

swelling over time was determined and compared to the complete DMEM supplemented with 100 ppm NaN_3 and 2 mM $CaCl_2$. Figure 15 displays the average bead volume over a 28-day period in both storage solutions. As expected, the storage medium supplemented with $CaCl_2$ resulted in little to no bead swelling compared to the storage medium without $CaCl_2$. However, the increase in average bead volume over time using the pure DMEM storage medium was also statistically insignificant ($p = 0.17$). The experiment should be repeated to draw stronger conclusions.

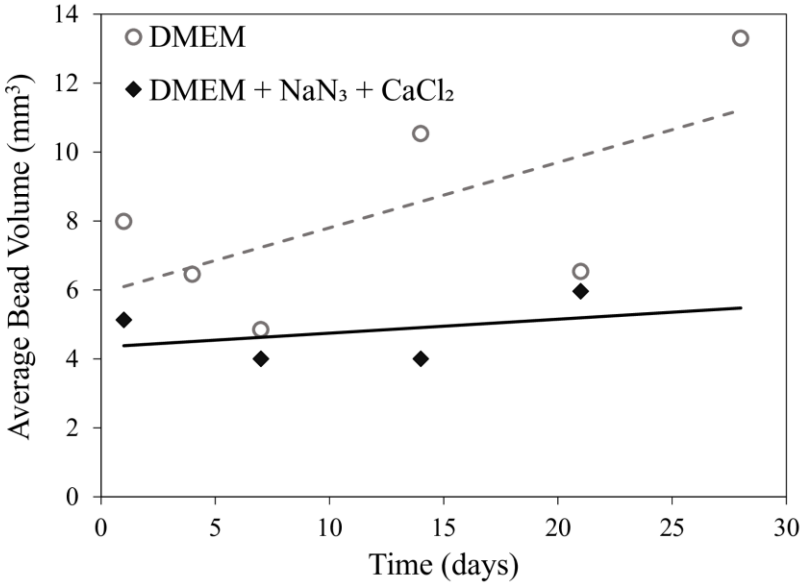

Figure 15. Effect of bead storage time in solutions with and without $CaCl_2$ on swelling. The trends were statistically insignificant, with $R^2 = 0.4071$ and $p = 0.17$ for the DMEM data and R^2 of 0.1348 and $p = 0.63$ for DMEM + 100 ppm NaN_3 + 2 mM $CaCl_2$ data.

Therefore, storage of alginate beads in complete DMEM or HEPES buffered saline solution, supplemented with 100 ppm NaN_3 and 2 mM $CaCl_2$ is advised for long-term capsule stability.

5.4.2 Mechanical and Physical Characteristics of Stirred and Microchannel Emulsification Alginate Beads

The mechanical properties and permeability of uncoated alginate beads depend on the polymer distribution and cross-linking density within the beads. Since the droplet formation mechanism, as well as the acidification and gelation kinetics were expected to be different between the microchannel and stirred emulsification processes, the resulting mechanical properties and permeability may be different. To test this hypothesis, we assessed the compressive rupture strength of both types of beads

and conducted permeability studies using inverse size exclusion chromatography. The beads produced using microchannel emulsification were shown to be stronger than those produced using stirred emulsification, with compressive burst strengths (average compressive force at 70% bead deformation) of 27.3 ± 0.4 g and 14 ± 1 g, respectively, as shown by the Texture Analyzer results (Figure 16). It is also evident that the compressive burst strength of the microchannel emulsification beads was more uniform compared to the stirred emulsification beads (much like the bead size uniformities), as shown by the similarities in the individual curves found in Figure 16B compared to Figure 16A.

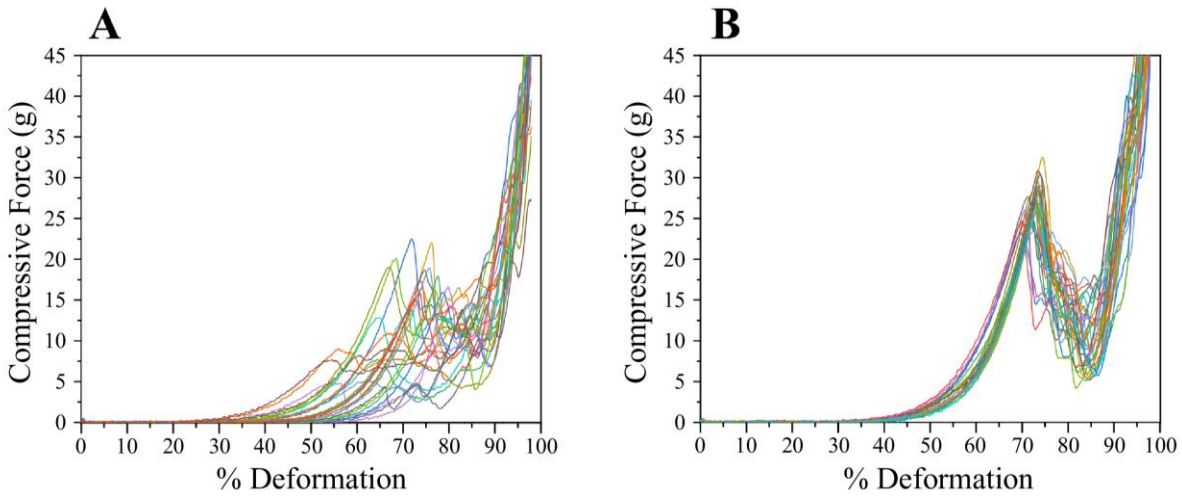

Figure 16. Compressive force as a function of bead deformation for alginate beads produced via emulsification processes.

A: Stirred emulsification microbead samples; **B:** Microchannel emulsification microbead samples. These graphs were generated by Igor Lacík, Dušana Treľová, and Zuzana Kroneková using a Texture Analyzer at the Polymer Institute of Slovak Academy of Sciences (Bratislava, Slovakia).

As determined from Figure 17A, the average molecular weight cut-off of the beads produced using microchannel emulsification (19 ± 2 kDa) was found to be slightly lower than that of the beads produced via stirred emulsification (43 ± 3 kDa). Figure 17B displays a slightly narrower curve for the beads produced using microchannel emulsification compared to stirred emulsification. Thus, microchannel emulsification resulted in beads with slightly smaller and more uniform pores than stirred emulsification.

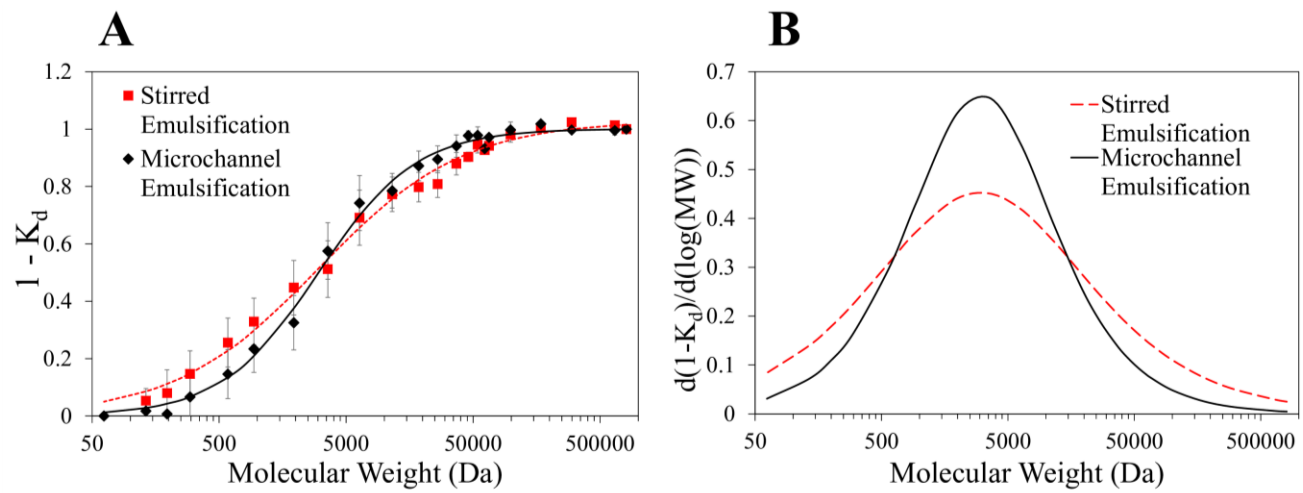

Figure 17. Permeability of alginate beads produced by stirred and microchannel emulsification processes measured by inverse size exclusion chromatography.

A: Influence of pullulan/dextran solute molecular weight on the volumetric fraction of the liquid volume in the pores from which the solute is excluded ($1 - K_d$), where K_d is the partition coefficient. Error bars represent standard error of n=3 runs. The s-shaped curves were fitted using the Boltzmann Equation 19 fitted to the data [117]. The MWCO represents the solute molecular weight at which $1 - K_d$ = 0.90 (i.e. 90% of the liquid volume inside the microbead pores excluded the solute). **B:** Derivative (slope) of the Boltzmann curves in A. A broader curve represents a broader pore size distribution.

As shown in the confocal Raman spectroscopy data (Figure 18), the alginate concentration was found to be homogeneous across the inner volume of both stirred emulsification and microchannel emulsification beads with slightly higher concentrations at the membrane surfaces. Figure 18 also displays that that the concentration of alginate was slightly higher in the microchannel emulsification beads (~1 wt% in the inner volume and ~1.5% at the bead surface) compared to the stirred emulsification beads (~0.8 wt% inner volume and ~1.1 wt% bead surface).

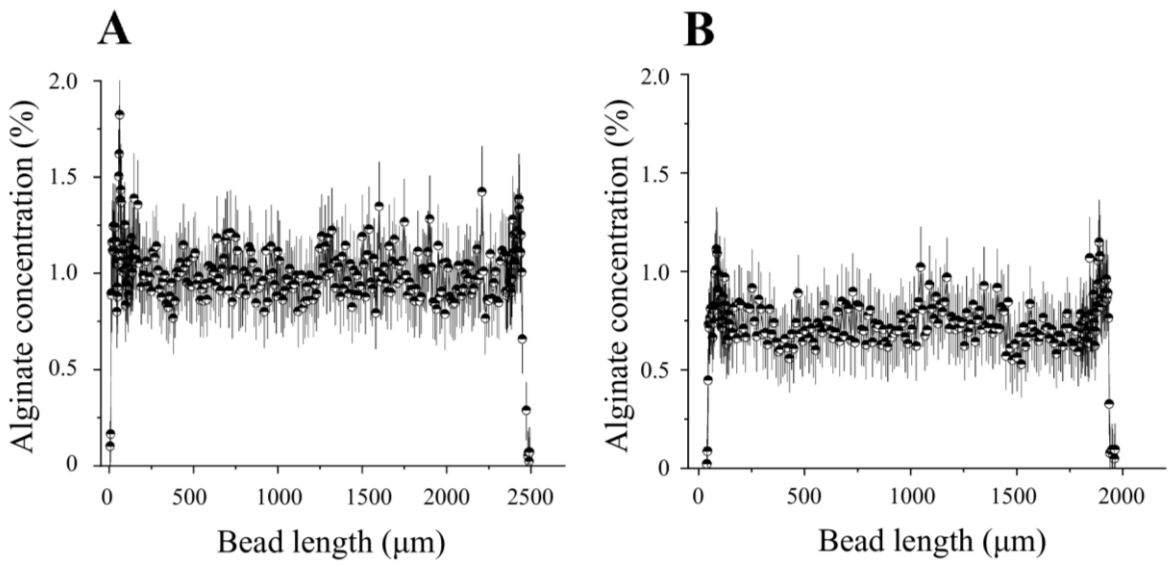

Figure 18. Concentration profile of alginate across the diameter of alginate microbeads produced via emulsification processes.

A: Microchannel emulsification microbead; **B:** Stirred emulsification microbead. The concentration profile was quantified by confocal Raman microscopy as previously described [99]. These graphs were generated by Igor Lacík, Dušana Treľová, and Zuzana Kroneková at the Polymer Institute of Slovak Academy of Sciences (Bratislava, Slovakia).

5.5 MIN6 Cell Survival Assessment

Once the microchannel emulsification device successfully produced uniform and spherical alginate beads, MIN6 cells were encapsulated to determine if mammalian cells can survive the process conditions. MIN6 cells were selected as a model pancreatic beta cell line as a first step towards future pancreatic islet cell encapsulation to treat diabetes. It was previously found that the acidification step in the stirred emulsification process led to the greatest drop in cell viability [49]. The acetic acid concentration in the microchannel emulsification process (0.22%) is higher than that in the stirred emulsification process (0.11%), which may potentially lead to a higher pH drop and increased cell death during the cell residence time in acidified oil. To minimize cell losses in the microchannel emulsification process, the time the alginate beads reside in the acidified continuous phase (acidification time) should be minimized. The minimum acidification time required for the 0.5%, 1.5% and 2.5% alginate beads to completely gel in the acidified continuous phase fluid was determined to be 2 minutes, as shown in Figure 19.

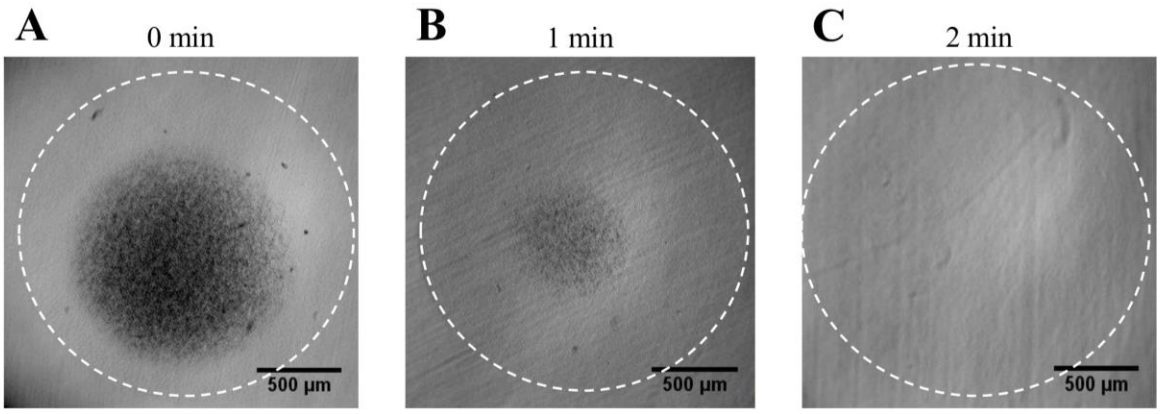

Figure 19. Effect of alginate droplet acidification time on observed $CaCO_3$ particle dissolution.

These 1.5% alginate beads were produced using the microchannel emulsification device and removed from the acidified continuous phase after various acidification times (**A:** 0 min; **B:** 1 min; **C:** 2 min). The dotted white line displays the bead contour. The central black dots are undissolved $CaCO_3$ particles, signifying an alginate droplet that is not fully gelled.

The viability of MIN6 cells encapsulated using the microchannel emulsification process with the minimum required acidification time of 2 minutes was then compared to the viabilities of cells after 4 and 10 minutes of acidification. As shown in Figure 20A and B, there was a significant effect of the bead residence time in acid on the encapsulated MIN6 cell viability, as expected, with the acidification time of 2 minutes showing the highest viability of ~61 ± 4%, and the acidification time of 10 minutes resulting in the lowest viability of ~27 ± 6%. The results shown in Figure 20C indicate that most of the cell death is attributed to the acidification process with a significant decrease in viability of ~37%. The droplet formation process prior to acid exposure resulted in an insignificant amount of cell death (<10%).

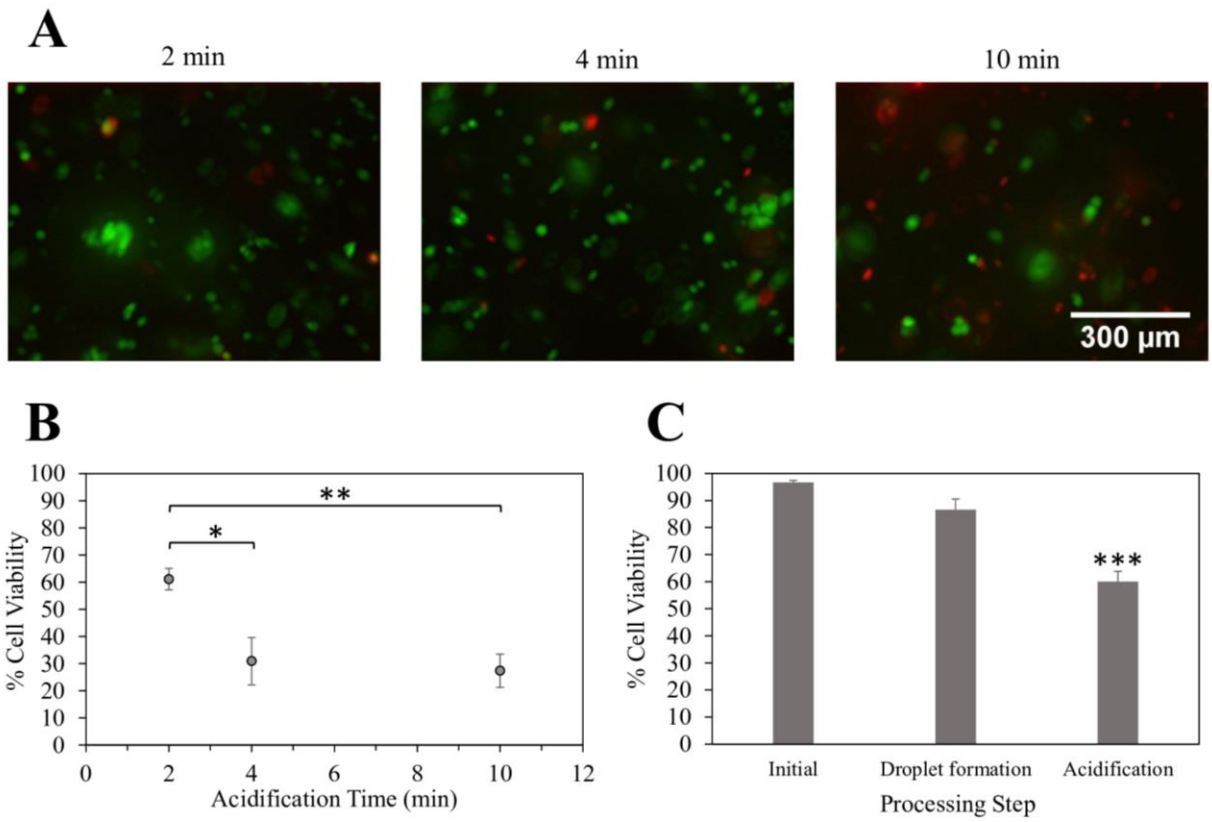

Figure 20. Effect of microchannel emulsification process steps and acidification time on MIN6 cell viability.

A: Effect of acidification time on cell survival visualized by calcein AM (live/green) and ethidium homodimer staining followed by fluorescence microscopy imaging at the microbead centers. **B:** Effect of acidification time on cell survival quantified by propidium iodide staining and flow cytometry. **C:** Cell viability measured by propidium iodide and flow cytometry after various microchannel emulsification processing steps (initial, droplet formation before acid exposure, and acidification/internal gelation). Error bars represent standard error of n=3 runs, *p<0.05 **p<0.01 ***p<0.001.

To determine whether the microchannel emulsification device can successfully encapsulate and maintain the viability of islet-like cell clusters, a preliminary encapsulation of MIN6 cell aggregates was conducted. Figure 21 displays the viability profile of an encapsulated MIN6 aggregate. The fluorescence microscope image shows that greater cell death occurred at the outer surface of the aggregate, with viable cells located in the inner aggregate volume. This result also provides a proof-of-concept that islet-like cell clusters can be encapsulated with the microchannel emulsification process.

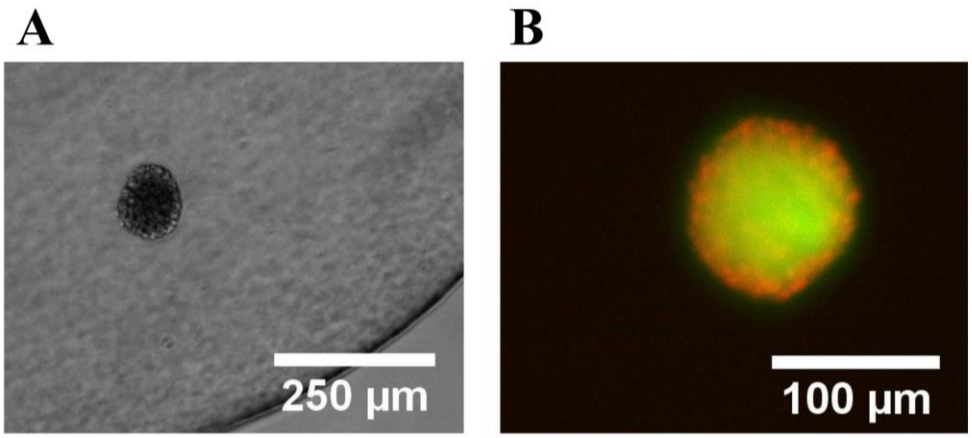

Figure 21. MIN6 cell aggregate encapsulated in an alginate microbead.
A: MIN6 cell aggregate immobilized in an alginate bead produced via microchannel emulsification; **B:** Fluorescence microscopy images taken after staining the bead in calcein AM (live/green cells) and ethidium homodimer (dead/red cells).

6 Discussion

In this study, a novel microchannel emulsification device that combines microchannel emulsification and internal gelation techniques was developed to produce monodisperse alginate beads for beta cell encapsulation. The effects of alginate flow rate and viscosity on bead diameter were studied and uniform beads ~1.5 to 2.5 mm in diameter were produced at rates up to 140 mL/h per channel.

The critical capillary number is useful in identifying the flow transition from droplet formation to jetting in the microchannel emulsification system [124]. Successful monodisperse alginate droplet generation was achieved for 0.5% to 2.5% alginate solution concentrations below the system's critical velocity using the heavy and low surface tension Novec^{TM} 7500 continuous phase fluid and a hydrophobic PTFE microchannel plate of high surface energy. Using the microchannel emulsification prototype, alginate viscosity was shown to have a significant positive correlation with bead diameter, increasing from ~1.7 mm to 2.3 mm in diameter for an alginate viscosity increase from ~0.005 Pa·s to 0.2 Pa·s. When viscous forces outweigh interfacial tension forces, droplet detachment slows down, resulting in larger droplets. On the other hand, alginate flow rate was shown to have an insignificant effect on bead diameter. This is consistent with the observation that interfacial tension and viscosity forces, the major forces governing microscale droplet formation below the critical capillary number, are independent of flow rate [125]. This signifies that the production rate of the process can be altered without an undesirable change in bead diameter.

However, increasing the flow rate past the system's critical capillary point resulted in jetting, or unstable droplet generation whereby the jet breaks up to form several polydisperse droplets [125]. The critical capillary number was shown to increase with alginate viscosity even though the alginate flow rate resulting in jetting had a decreasing trend. This occurred because the increase in viscosity outweighed the effect of flow rate on jetting. The absolute values for the critical capillary numbers calculated may change depending on the actual measured interfacial tension; however, the trend would likely remain as the trend was highly significant. The calculated critical capillary number at an alginate concentration of 1.5% (0.39 ± 0.04) was similar to literature values of 0.3 [126]. To favor droplet formation by increasing the instability of the interface, the

viscosity within the microchannel is desired to be the lowest possible therefore decreasing the capillary number [127]. This can be attained by increasing the temperature [113, 121] or by using a dispersed phase of lower viscosity. Alternatively, surfactants can be used to reduce the interfacial tension between the dispersed and continuous phases, resulting in smaller alginate droplets [128].

The microchannel emulsification device produced 0.5%, 1.5% and 2.5% alginate beads much more uniform in size compared to those produced using the stirred emulsification process. Contrary to stirred emulsification, where droplet diameter depends on the energy dissipation at various distances from the impellor tip [49], microchannel emulsification droplet generation encompasses a spontaneous droplet generation mechanism that only depends on viscous and interfacial tension forces, both of which are fluid dependent. Thus, most of the droplets produced from a given alginate concentration via microchannel emulsification are uniform in size. Still, it can be noted that a few smaller beads were produced randomly as shown in Figure 13A which cause the coefficient of variation to reach 10%. These smaller beads are a result of short periods of unstable droplet generation, which may have resulted from sudden spikes in fluid velocity following pressurized unblocking of fouled microchannels. This case occurred rarely in our process, allowing the coefficient of variation of the alginate beads to remain relatively low.

Besides bead uniformity, the mechanical stability of alginate beads is another essential characteristic that determines the success or failure of long-term storage of manufactured beads. The mechanical integrity of the beads should be maintained over time in case of delays in characterization testing, or long-distance transportation of the product at the manufacturing stage. The optimal storage solution for long-term storage of alginate beads was determined to be complete DMEM or HEPES buffered saline solution supplemented with 100 ppm NaN_3 and 2 mM $CaCl_2$. HEPES buffered saline solution was the selected buffer solution because it has low metal chelating capability compared to other phosphate-containing buffers (e.g. phosphate buffered saline). Chelators are undesirable as they have a high affinity for divalent cations such as Ca^{2+} and would ultimately lead to de-crosslinking of the alginate gel. However, without $CaCl_2$, the monovalent cations (such as Na^+) in the HEPES buffered saline solution undergo ion-exchange with the Ca^{2+} ions that are binding the carboxyl groups in the gelled alginate matrix. This results in electrostatic repulsion among the ionized carboxyl groups, leading to bead swelling, after which

bead degradation occurs as Ca^{2+} ions diffuse out of the beads into the surrounding storage medium [111].

The capsules should also show enough strength to be able to withstand any shear forces that may occur during the implantation process [93] to avoid microcapsule breaking and subsequent inflammation. The compression modulus and shear modulus of alginate hydrogels typically range from 1 to >1000 kPa, and 0.02 to 40 kPa, respectively [129]. The beads produced using microchannel emulsification were found to be stronger than those using stirred emulsification (compressive burst strengths of 27.3 ± 0.4 g and 14 ± 1 g, respectively). The main reason for this result was likely that the microchannel emulsification beads were slightly larger, indicating that larger beads withstand higher compressive load. To further support this, the compressive burst strength of the stirred emulsification beads (average diameter of ~2190 μm) was higher than the previously reported compressive burst strength for smaller 1.5% alginate beads (average diameter of ~700 μm) produced via the same stirred emulsification process (~0.5 g) [14]. This means that once smaller beads are produced using the microchannel emulsification device, the mechanical strength might be compromised. However, the peak force at burst for alginate beads being transplanted in the peritoneal cavity and subcutaneous space of rats was reported to be as low as 0.91 g [130], meaning there is ample room for a reduced compressive burst strength as a result of reduced microchannel emulsification bead diameter.

Furthermore, during the rinse process, the beads are exposed to HEPES buffered saline solution with 10% complete DMEM, which may lead to a decrease in the bead mechanical strength due to the presence of monovalent cations (Na^{+}) in the solution, which compete with the Ca^{2+} cross-links. This problem can be resolved by adding 2 mM $CaCl_2$ to the rinsing solution. Another method to improve bead mechanical strength would involve using an alginate powder with a higher G:M subunit ratio [12]. Thus, several methods exist to further improve the mechanical stability of the beads produced via microchannel emulsification and stirred emulsification. On the other hand, studies have shown that the stability of beads depends more on the transplant site rather than the bead properties, with improved stability in the stratium and subcutaneous space compared to the peritoneal cavity due to differences in the presence of harmful enzymes (e.g. amylase, maltase, β-glucuronidase) leading to bead degradation [93]. Therefore, the transplantation site must be carefully considered along with inherent mechanical properties of the microbeads.

Characterizing the permeability and concentration profile of our pure alginate beads for islet encapsulation is also useful to predict the diffusion behaviour of insulin, nutrients, oxygen, antibodies, and immune cells across the porous alginate microcapsules. Alginate bead pore diameters depend on alginate concentration, alginate formulation, and $CaCO_3$ concentration. Microchannel emulsification beads showed smaller and more uniform pores than the beads generated by stirred emulsification (MWCO of 19 ± 2 kDa and 43 ± 3 kDa, respectively), although both processes utilized the same $CaCO_3$ concentration (0.05 vol%), alginate formulation and alginate concentration (1.5%). This result suggests that the stirred emulsification process likely led to swelling of the beads, which was further confirmed by the reduced concentration profile in the stirred emulsification beads (~0.8% to 1.1%) compared to the microchannel emulsification beads (~1% to 1.5%) in the Raman spectroscopy analysis (Figure 18). The stirred emulsification bead swelling is possibly due to the time the beads were exposed to the Na^+ ion-containing rinsing solution (~10 min) compared to the microchannel emulsification process (<5 min). Interestingly, the MWCO achieved in both processes was smaller than the 150 kDa immunoglobulin G (IgG) antibodies [131], unlike the MWCO obtained for uncoated beads produced using electrostatic nozzle encapsulation and external gelation (~77 kDa to 600 kDa) [131-133]. Therefore, successful immunoisolation of islets encapsulated using stirred emulsification or microchannel emulsification is promising.

The use of Ba^{2+} instead of Ca^{2+} as a cross-linker would lead to increased gel strength and stability, decreased alginate bead size, reduced bead swelling, and reduced permeability to IgG, for alginate with high-G content [47]. However, the opposite trend is expected for high-M alginate, as observed in literature [134], and Ba^{2+} ions are more toxic than Ca^{2+} ions [135]. Alternatively, the mechanical stability of the alginate beads can be improved by coating alginate beads with poly-cations (e.g. chitosan or poly-L-lysine). These polycation coatings reduce permeability and are stable in the presence of monovalent ions as well as Ca^{2+}-chelating agents [136]. Furthermore, these coatings would enable the use of lower viscosity alginate solutions without compromising permeability, which is preferable to minimize the shear stress imparted on cells during the encapsulation process. However, previous studies have shown that the addition of external polycation coatings on beads leads to increased fibrotic overgrowth due to the increased zeta potential of the positively-charged surface [137].

Other than the viscous forces applied to the encapsulated cells, other factors affect the viability of these cells in the microchannel emulsification encapsulation process. Increasing the bead residence time in the acidified continuous phase resulted in a decrease in MIN6 cell viability because the H^+ ions had more time to permeate through the microcapsules causing a decrease in the pH exposed to the cells. Reducing the bead residence time in acid to the minimum value of 2 minutes resulted in a maximum cell viability of ~60%. This value is much lower than the cell viability obtained using stirred emulsification (~90%), most likely because the microchannel emulsification process utilizes a higher acetic acid concentration (0.22 vol%) than the stirred emulsification process (0.11 vol%). Most of the cell death in the microchannel emulsification process was due to the acidification step (loss of 37%), with a loss of only 10% of cells during the droplet formation process, suggesting that a reduction in the acetic acid concentration should lead to significant improvements in cell viability, which was shown in stirred emulsification viability studies [49]. Encapsulation and viability assessment of MIN6 aggregates also confirmed this conclusion as the cells at the aggregate surface showed greater cell death than those in the inner volume likely because the H^+ ions would have reached the aggregate surface first.

Unlike previous microchannel emulsification processes, this novel device can form a water-in-oil emulsion whereby simultaneous emulsification and internal gelation processes result in uniform gelled alginate beads encapsulating cells. The process parameters currently achieved by the microchannel emulsification device, including production rate, alginate viscosity operation range, compressive load at bead rupture, permeability (MWCO), bead diameter, bead diameter coefficient of variation, and encapsulated cell viability compared to those attained by conventional nozzle and stirred emulsification encapsulation devices are summarized in Table 6. The device can overcome the challenges associated with conventional nozzle encapsulation devices, including reaching clinical scale production rates with merely six microchannels in parallel, without substantially increasing complexity of the process. Moreover, the device produces droplets much more uniform in diameter than those produced using stirred emulsification.

Table 6. Current alginate bead encapsulation process production rates, bead diameters, bead size uniformity and operable viscosity range compared to target values.

Process	Maximum Production Rate (mL/h)	Alginate Viscosity Range (Pa·s)	Compressive Load (mN)	MWCO (kDa)	Bead Diameter (μm)	Cell Viability	Coefficient of Variation	References
Nozzle Vibrating	1,250	< 0.2	30	150	300 - 5,000	97%	<10%	[14, 43, 47, 138]
Nozzle Electrostatic	60	< 0.7	30	150	300 - 5,000	97%	<10%	[45, 139]
Nozzle JetCutter	2,000	< 11	30	150	>200	97%	<10%	[46, 47]
Stirred Emulsification	$> 10^6$	< 112	5 - 30	20 - 207	200 - 2,000	90%	40 - 60%	[14, 49, 50]
Microchannel Emulsification	140 (per channel)	< 0.2	27	17 - 20	1,500 - 3,000	57 - 65%	< 10%	[16]
Target	100	2 - 3	>30	<150	600	>95%	< 10%	[13, 14]

However, being a continuous process with microchannel confinement, microchannel emulsification is a slightly more complex process than stirred emulsification and simple nozzle encapsulators, with challenges in bead size reduction, potential leaking, microchannel fouling or obstruction, and cell death. Channel obstruction will likely be a common occurrence with cell aggregate encapsulations since the size of aggregates (~150 μm) was very close to the smallest channel dimension (~180 μm). In our preliminary aggregate encapsulation studies, only one aggregate was located during imaging suggesting that most of aggregates did not pass through the microchannels. Since our channels were tapered, the aggregates likely entered the channel easily and had difficulties leaving from the exit that was narrower. This would have led to the accumulation of aggregates in the microchannel, resulting in problematic channel obstruction.

The microchannel emulsification device has the flexibility to reach a wide variety of applications aside from islet transplantation and type 1 diabetes treatment. The fact that it can

function over a wide range of alginate viscosities means that the permeability of the microcapsule can be tuned to fit the application, whether it be for controlled release of microorganisms in agriculture applications, effective and safe delivery of active components through the skin in cosmetic applications, masking unpleasant tastes and burning sensations in certain foods, or immunoisolation of tissues or biological active substances in regenerative medicine and cellular therapy.

7 Recommendations for Future Work

Successful development of the microchannel emulsification device was achieved in many aspects including the generation of uniform proof-of-concept microbeads at clinical scale production rates (>100 mL/h per microchannel) over a wide alginate viscosity operating range (0.005 to 0.2 Pa·s).

There is still work to be done to achieve average bead diameters closers to the target of 600 µm and to increase encapsulated cell viability ideally to >95%. Strategies to further decrease the bead diameter could be to add surfactants to the continuous and dispersed phase fluids. Surfactants are expected to decrease the interfacial tension between the dispersed and continuous phases, resulting in smaller droplets [128]. Preliminary tests have shown a significant reduction in alginate bead diameter with surfactants. Reducing the bead size will not only reduce oxygen diffusion limitations in the capsule but should also result in a lower concentration of acetic acid required for complete bead gelation. Reduced acid content could improve both immediate and long-term viability of encapsulated cells. Therefore, further experiments with surfactants may solve bead size and cell viability issues, two of the major concerns with our current device.

To further understand and predict the effects of various process variables (e.g. interfacial tension, density, flow rate, viscosity and temperature) on droplet diameter and formation rate, a computer model that simulates water-in-oil emulsion formation and gelation using our microchannel emulsification device could be developed. The model would be based on the balance of interfacial tension, buoyancy, inertial and viscous forces acting on the alginate liquid as it exits the microchannels. Unlike models already found in literature [78, 140], the model would be for a water-in-oil emulsion produced using rectangular oblong straight-through (and tapered) microchannels. Existing models are for elliptical or round straight-through microchannels [78], or terrace microchannel systems [140].

Development of microchannel plate storage techniques and microchannel cleaning processes could also be done to reduce and/or remove fouling in the microchannel plate. This would avoid microchannel blockage and periods of unstable bead generation. For instance, storing the microchannel plate in oil between trials may reduce the risk of bacterial growth in the channels

with time. Furthermore, filtering the alginate prior to use is recommended to avoid the presence of particles larger than the channels that may obstruct dispersed phase flow.

Further process modifications might also include adding an outlet from the collection chamber such that the beads can flow out of the device continuously into a rinsing fluid (complete DMEM) and creating an inlet continuous flow of the acidified oil phase to replenish the acetic acid content. To test the scalability of the device, the use of microchannel plates with more than three microchannels in parallel should be attempted. This scale-up step may be challenging as the microdroplets produced in parallel may contact each other and coalesce before gelling. The use of $BaCO_3$ instead of $CaCO_3$ in the alginate phase and its impact on bead strength and permeability could also be tested in the future. We hypothesize that $BaCO_3$ will lead to stronger beads with smaller pores [28, 31-33].

The hope of pursuing this future work would be to develop a continuous clinical-scale process that can immobilize pancreatic beta cells in a mechanically durable material without impacting function and long-term viability of cells.

8 Conclusions

Pancreatic islet cell immobilisation and transplantation has shown great promise in the biomedical field as a potential treatment option for type 1 diabetes. This technique has the potential to eliminate the periodic requirement of insulin injections by providing a method for introducing insulin-producing cells into the body without rejection by the immune system. Recent research has enabled the development of several cell encapsulation techniques with alginate-based materials, including nozzle-based encapsulation, and stirred emulsification. Microchannel emulsification is a novel and attractive option for producing alginate-encapsulated islets at high production rates and controlled sizes. Compared with the standard nozzle-based encapsulators, microchannel emulsification can more readily be scaled to clinically and even industrially-relevant throughputs without significantly increasing process complexity. Furthermore, the beads produced using microchannel emulsification are much more uniform in size than those obtained from stirred emulsification.

The objective of this work was to optimize and characterize a novel microchannel emulsification device to achieve control over the bead size, uniformity, mechanical stability, permeability, and viability of encapsulated beta cells. This work demonstrated the following:

1) 3M^{TM} Novec^{TM} 7500 Engineered Fluid is a promising continuous phase fluid to promote alginate droplet formation by microchannel emulsification due to its low surface tension (~0.0158 N/m) and high density difference with the to-be-dispersed alginate phase ~615 ± 4 kg/m^3;
2) Polytetrafluoroethylene (PTFE) was the selected microchannel plate material because of its hydrophobicity and high surface free energy (~28 ± 1 mJ/m^2), which would promote microchannel wetting by the continuous phase fluid and the resultant formation of the droplet neck required for spontaneous droplet detachment;
3) Increasing the alginate phase flow rate up to a critical value increased production rates without significantly influencing bead diameter, confirming previous observations for other microchannel emulsification systems;

4) Exceeding the critical alginate flow rate resulted in elongated droplet formation (necking) followed by continuous outflow of the dispersed phase through the microchannel (jetting);
5) The system critical capillary numbers ranged from ~0.08 ± 0.02 to 0.51 ± 0.08 for alginate solution viscosities from ~0.005 to 0.2 Pa·s;
6) Increasing the viscosity of alginate from 0.005 to 0.2 Pa·s also increased the bead diameter from ~1.7 to ~2.3 mm;
7) The beads produced via microchannel emulsification were consistently uniform with a coefficient of variation usually <10%, unlike stirred emulsification which resulted in beads of much higher coefficients of variation of >60%;
8) The microchannel emulsification beads had higher compressive burst strength (27.3 ± 0.4 g) and lower permeability (MWCO of 19 ± 2 kDa) compared to the stirred emulsification beads (14 ± 1 g and 43 ± 3 kDa, respectively).
9) The microchannel emulsification beads also displayed higher alginate concentrations across the bead radius (~1% to 1.5%) compared to the stirred emulsification beads (~0.8% to 1.1%) possibly due to swelling of the stirred emulsification beads during the >10-min rinsing step;
10) The viability of MIN6 cells showed an increasing trend with a decrease in the bead residence time in acidified continuous phase up to a value of ~60%;
11) 37% of the cell losses was due to acidification and internal gelation in the microchannel emulsification process, with <10% losses due to droplet formation through the microchannel.

Major improvements in the viability of encapsulated cells is required and can be achieved by decreasing the acid concentration in the continuous phase fluid. Further experiments are also required to achieve bead diameters closer to ~600 μm specifically for the application of islet immobilization and implantation. This will likely be achieved by adding surfactants in both continuous and dispersed phases. However, the current bead diameter range achieved can be useful for a variety of other applications in food and cosmetic industries, including the encapsulation of flavouring agents in food products [141], or the cryopreservation of plant germplasm [142], both of which may require beads ranging from 1.5 mm to 5 mm in diameter. Furthermore, a study showed that larger beads close to the size we are achieving (1.5 mm) were more mechanically

stable *in vivo* with significantly reduced fibrosis compared to smaller 0.5 mm alginate beads [143]. This signifies that these larger beads may be promising for various drug and cell delivery applications.

The novel microchannel emulsification device provides a versatile platform for the development of cell encapsulation processes tailored for applications ranging from cellular therapy, drug delivery [144], preservation of bioactive food components [145], meat preservation [146], agriculture [1] and cosmetics [147]. Its versatility stems from its capability to produce a broad range of bead diameters (1.5 mm to 5 mm) using a wide range of polymer viscosities, leading to hydrogel microbeads with tunable permeabilities. The device also has a high scale-up potential with room for adding several microchannels in parallel. For these reasons, alginate microbead generation using the microchannel emulsification device has the potential to solve numerous commercial and research problems currently encountered in fields including medicine, food and biotechnology.

9 References

1. Schoebitz, M., M.D. López, and A. Roldán, *Bioencapsulation of microbial inoculants for better soil–plant fertilization. A review.* Agronomy for sustainable development, 2013. **33**(4): p. 751-765.
2. Soon-Shiong, P., *Treatment of type I diabetes using encapsulated islets1.* Advanced drug delivery reviews, 1999. **35**(2-3): p. 259-270.
3. Liu, X., et al., *Engineering β-cell islets or islet-like structures for type 1 diabetes treatment.* Medical hypotheses, 2015. **85**(1): p. 82-84.
4. Siebers, U., et al., *Alginate-based Microcapsules for Immunoprotected Islet Transplantation.* Annals of the New York Academy of Sciences., 1998. **831**: p. 304.
5. Bergenstal, R.M., et al., *Effectiveness of sensor-augmented insulin-pump therapy in type 1 diabetes.* New England Journal of Medicine, 2010. **363**(4): p. 311-320.
6. Krishnan, R., et al., *Islet and stem cell encapsulation for clinical transplantation.* The review of diabetic studies: RDS, 2014. **11**(1): p. 84.
7. Hirshberg, B., *Lessons learned from the international trial of the edmonton protocol for islet transplantation.* Current diabetes reports, 2007. **7**(4): p. 301-303.
8. Shapiro, A.J., et al., *Islet transplantation in seven patients with type 1 diabetes mellitus using a glucocorticoid-free immunosuppressive regimen.* New England Journal of Medicine, 2000. **343**(4): p. 230-238.
9. Shapiro, A.M., M. Pokrywczynska, and C. Ricordi, *Clinical pancreatic islet transplantation.* Nat Rev Endocrinol, 2017. **13**(5): p. 268-277.
10. Dufrane, D. and P. Gianello, *Macro-or microencapsulation of pig islets to cure type 1 diabetes.* World journal of gastroenterology: WJG, 2012. **18**(47): p. 6885.
11. de Vos, P., et al., *Long-term biocompatibility, chemistry, and function of microencapsulated pancreatic islets.* Biomaterials, 2003. **24**(2): p. 305-312.
12. de Vos, P., et al., *Alginate-based microcapsules for immunoisolation of pancreatic islets.* Biomaterials, 2006. **27**(32): p. 5603-17.
13. Fernandez, S., *Emulsion-based islet encapsulation: predicting and overcoming islet hypoxia*. Bioencapsulation Innovations, 2014. **220**: p. 14-15.
14. Hoesli, C.A., et al., *Reversal of diabetes by betaTC3 cells encapsulated in alginate beads generated by emulsion and internal gelation.* J Biomed Mater Res B Appl Biomater, 2012. **100**(4): p. 1017-28.
15. Hoesli, C., *Bioprocess development for the cell-based treatment of diabetes*. 2010, University of British Columbia.
16. Markwick, K., *Alginate microbead production for diabetes cellular therapy*. 2016, McGill University.
17. Neufeld, T., et al., *The efficacy of an immunoisolating membrane system for islet xenotransplantation in minipigs.* PloS one, 2013. **8**(8): p. e70150.
18. Rotem, A., et al., *Oxygen supply for cell transplant and vascularization*. 2013, Google Patents.
19. Agulnick, A.D., et al., *Insulin-producing endocrine cells differentiated in vitro from human embryonic stem cells function in macroencapsulation devices in vivo.* Stem cells translational medicine, 2015. **4**(10): p. 1214-1222.

20. Trivedi, N., et al., *Improved vascularization of planar membrane diffusion devices following continuous infusion of vascular endothelial growth factor.* Cell transplantation, 2000. **9**(1): p. 115-124.
21. Dufrane, D., et al., *The influence of implantation site on the biocompatibility and survival of alginate encapsulated pig islets in rats.* Biomaterials, 2006. **27**(17): p. 3201-3208.
22. Desai, N., et al., *Interpenetrating polymer networks of alginate and polyethylene glycol for encapsulation of islets of Langerhans.* Journal of microencapsulation, 2000. **17**(6): p. 677-690.
23. Wang, D., et al., *Encapsulation of plasmid DNA in biodegradable poly (D, L-lactic-co-glycolic acid) microspheres as a novel approach for immunogene delivery.* Journal of Controlled Release, 1999. **57**(1): p. 9-18.
24. Shoichet, M.S., et al., *Stability of hydrogels used in cell encapsulation: An in vitro comparison of alginate and agarose.* Biotechnology and bioengineering, 1996. **50**(4): p. 374-381.
25. Sefton, M.V., et al., *Microencapsulation of mammalian cells in a water-insoluble polyacrylate by coextrustion and interfacial precipitation.* Biotechnology and bioengineering, 1987. **29**(9): p. 1135-1143.
26. Mørch, Ý.A., *Novel alginate microcapsules for cell therapy.* Department of Biotechnology, 2008.
27. Choi, C.-H., et al., *Generation of monodisperse alginate microbeads and in situ encapsulation of cell in microfluidic device.* Biomedical microdevices, 2007. **9**(6): p. 855-862.
28. Smidsrød, O., *Molecular basis for some physical properties of alginates in the gel state.* Faraday discussions of the Chemical Society, 1974. **57**: p. 263-274.
29. Donati, I., et al., *New Hypothesis on the Role of Alternating Sequences in Calcium−Alginate Gels.* Biomacromolecules, 2005. **6**(2): p. 1031-1040.
30. Thu, B., et al., *Alginate polycation microcapsules: I. Interaction between alginate and polycation.* Biomaterials, 1996. **17**(10): p. 1031-1040.
31. Bajpai, S.K. and S. Sharma, *Investigation of swelling/degradation behaviour of alginate beads crosslinked with Ca2+ and Ba2+ ions.* Reactive and Functional Polymers, 2004. **59**(2): p. 129-140.
32. Mørch, Ý.A., I. Donati, and B.L. Strand, *Effect of Ca2+, Ba2+, and Sr2+ on Alginate Microbeads.* Biomacromolecules, 2006. **7**(5): p. 1471-1480.
33. Smidsrød, O. and G. Skja˚k-Br҆k, *Alginate as immobilization matrix for cells.* Trends in Biotechnology, 1990. **8**: p. 71-78.
34. Zimmermann, U., et al., *Hydrogel-based non-autologous cell and tissue therapy.* Biotechniques, 2000. **29**(3): p. 564-581.
35. Hillgärtner, M., et al., *Immunoisolation of transplants by entrapment in 19F-labelled alginate gels: production, biocompatibility, stability, and long-term monitoring of functional integrity.* Materialwissenschaft und Werkstofftechnik: Entwicklung, Fertigung, Prüfung, Eigenschaften und Anwendungen technischer Werkstoffe, 1999. **30**(12): p. 783-792.
36. Skjåk-Bræk, G., E. Murano, and S. Paoletti, *Alginate as immobilization material. II: Determination of polyphenol contaminants by fluorescence spectroscopy, and evaluation of methods for their removal.* Biotechnology and bioengineering, 1989. **33**(1): p. 90-94.

37. Serp, D., et al., *Characterization of an encapsulation device for the production of monodisperse alginate beads for cell immobilization.* Biotechnology and Bioengineering, 2000. **70**(1): p. 41-53.
38. Leo, W.J., A.J. McLoughlin, and D.M. Malone, *Effects of sterilization treatments on some properties of alginate solutions and gels.* Biotechnology Progress, 1990. **6**(1): p. 51-53.
39. Daigle, D.J. and P.J. Cotty, *The Effect of Sterilization, pH, Filler and Spore Inoculum Concentration on the Preparation of Alginate Pellets.* Biocontrol Science and Technology, 1997. **7**(1): p. 3-10.
40. Brandenberger, H., et al., *Monodisperse particle production: A method to prevent drop coalescence using electrostatic forces.* Journal of Electrostatics, 1999. **45**(3): p. 227-238.
41. Serp, D., et al., *Characterization of an encapsulation device for the production of monodisperse alginate beads for cell immobilization.* Biotechnology and bioengineering, 2000. **70**(1): p. 41-53.
42. Schwinger, C., et al., *High throughput encapsulation of murine fibroblasts in alginate using the JetCutter technology.* Journal of Microencapsulation, 2002. **19**(3): p. 273-280.
43. Steele, J.A.M., et al., *Therapeutic cell encapsulation techniques and applications in diabetes.* Advanced Drug Delivery Reviews, 2014. **67-68**: p. 74-83.
44. Klokk and Melvik, *Controlling the size of alginate gel beads by use of a high electrostatic potential.* Journal of Microencapsulation, 2002. **19**(4): p. 415-424.
45. Lewinska, D., et al., *Electrostatic microencapsulation of living cells.* Biocybernetics and Biomedical Engineering, 2008. **28**(2): p. 69-85.
46. Prusse, U., et al., *K.D Vorlop, Bead Production with JetCutting and Rotating Disc/Nozzle Technologies*. 2002. 1-10.
47. Koch, S., et al., *Alginate encapsulation of genetically engineered mammalian cells: Comparison of production devices, methods and microcapsule characteristics.* Journal of Microencapsulation, 2003. **20**(3): p. 303-316.
48. Hoesli, C.A., M. Luu, and J.M. Piret, *A novel alginate hollow fiber bioreactor process for cellular therapy applications.* Biotechnol Prog, 2009. **25**(6): p. 1740-51.
49. Hoesli, C.A., et al., *Pancreatic Cell Immobilization in Alginate Beads Produced by Emulsion and Internal Gelation.* Biotechnology and Bioengineering, 2011. **108**(2): p. 424-434.
50. Poncelet, D., et al., *Production of alginate beads by emulsification/internal gelation. I. Methodology.* Appl Microbiol Biotechnol, 1992. **38**(1): p. 39-45.
51. Reis, C.P., et al., *Review and current status of emulsion/dispersion technology using an internal gelation process for the design of alginate particles.* JOURNAL OF MICROENCAPSULATION, 2006. **23**(3): p. 245-257.
52. Nedović, V. and R. Willaert, *Applications of cell immobilisation biotechnology*. 2005, Springer: Dordrecht ;.
53. Chan, L.W., H.Y. Lee, and P.W.S. Heng, *Mechanisms of external and internal gelation and their impact on the functions of alginate as a coat and delivery system.* Carbohydrate Polymers, 2006. **63**(2): p. 176-187.
54. McClements, D.J., *Food emulsions: principles, practices, and techniques*. 2015: CRC press.
55. Sugiura, S., et al., *Size control of calcium alginate beads containing living cells using micro-nozzle array.* Biomaterials, 2005. **26**(16): p. 3327-3331.

56. Lim, F. and A.M. Sun, *Microencapsulated islets as bioartificial endocrine pancreas.* Science, 1980. **210**(4472): p. 908-910.
57. Sun, Y., et al., *Normalization of diabetes in spontaneously diabetic cynomologus monkeys by xenografts of microencapsulated porcine islets without immunosuppression.* The Journal of clinical investigation, 1996. **98**(6): p. 1417-1422.
58. Soon-Shiong, P., et al., *Insulin independence in a type 1 diabetic patient after encapsulated islet transplantation.* Lancet (London, England), 1994. **343**(8903): p. 950-951.
59. Calafiore, R., et al., *Microencapsulated pancreatic islet allografts into nonimmunosuppressed patients with type 1 diabetes: first two cases.* Diabetes care, 2006. **29**(1): p. 137-138.
60. Omer, A., et al., *Long-term normoglycemia in rats receiving transplants with encapsulated islets.* Transplantation, 2005. **79**(1): p. 52-8.
61. Tan, P.L., *Company profile: tissue regeneration for diabetes and neurological diseases at living cell technologies.* Regenerative medicine, 2010. **5**(2): p. 181-187.
62. Elliott, R., et al. *Intraperitoneal alginate-encapsulated neonatal porcine islets in a placebo-controlled study with 16 diabetic cynomolgus primates*. in *Transplantation proceedings*. 2005. Elsevier.
63. Nakashima, T., M. Shimizu, and M. Kukizaki, *Particle control of emulsion by membrane emulsification and its applications.* Advanced Drug Delivery Reviews, 2000. **45**(1): p. 47-56.
64. Charcosset, C. and H. Fessi, *MEMBRANE EMULSIFICATION AND MICROCHANNEL EMULSIFICATION PROCESSES,* in *Reviews in Chemical Engineering*. 2005. p. 1.
65. Sugiura, S., et al., *Interfacial Tension Driven Monodispersed Droplet Formation from Microfabricated Channel Array.* Langmuir, 2001. **17**(18): p. 5562-5566.
66. Kawakatsu, T., et al., *Production of Monodispersed Oil-in-Water Emulsion Using Crossflow-Type Silicon Microchannel Plate.* JOURNAL OF CHEMICAL ENGINEERING OF JAPAN, 1999. **32**(2): p. 241-244.
67. Kobayashi, I., M. Nakajima, and S. Mukataka, *Preparation characteristics of oil-in-water emulsions using differently charged surfactants in straight-through microchannel emulsification.* Colloids and Surfaces a-Physicochemical and Engineering Aspects, 2003. **229**(1-3): p. 33-41.
68. Dijke, v.K.C., et al., *Effect of viscosities of dispersed and continuous phases in microchannel oil-in-water emulsification.* Microfluidics and Nanofluidics, 2010. **9**(1): p. 77-85.
69. Kobayashi, I., S. Mukataka, and M. Nakajima, *Effect of slot aspect ratio on droplet formation from silicon straight-through microchannels.* Journal of Colloid and Interface Science, 2004. **279**(1): p. 277-280.
70. Butron Fujiu, K., et al., *Temperature effect on microchannel oil-in-water emulsification*. Vol. 10. 2010. 773-783.
71. Kobayashi, I., et al., *CFD analysis of microchannel emulsification: Droplet generation process and size effect of asymmetric straight flow-through microchannels.* Chemical Engineering Science, 2011. **66**(22): p. 5556-5565.
72. Timgren, A., G. Trägårdh, and C. Trägårdh, *Application of the PIV technique to measurements around and inside a forming drop in a liquid-liquid system.* Experiments in Fluids : Experimental Methods and their Applications to Fluid Flow, 2008. **44**(4): p. 565-575.

73. Kobayashi, I., et al., *Generation of uniform drops via through-hole arrays micromachined in stainless-steel plates.* Microfluidics and Nanofluidics, 2008. **5**(5): p. 677-687.
74. De Luca, G., et al., *Modelling droplet formation in cross-flow membrane emulsification.* Desalination, 2006. **199**(1): p. 177-179.
75. Kobayashi, I., K. Uemura, and M. Nakajima, *Effects of channel and operation parameters on emulsion production using oblong straight-through microchannels.* Japan Journal of Food Engineering, 2009. **10**(1): p. 69-75.
76. van der Zwan, E., K. Schroën, and R. Boom, *A Geometric Model for the Dynamics of Microchannel Emulsification.* Langmuir, 2009. **25**(13): p. 7320-7327.
77. Wu, L. and Y. Chen, *Visualization study of emulsion droplet formation in a coflowing microchannel.* Chemical Engineering & Processing: Process Intensification, 2014. **85**: p. 77-85.
78. Kobayashi, I., S. Mukataka, and M. Nakajima, *CFD Simulation and Analysis of Emulsion Droplet Formation from Straight-Through Microchannels.* Langmuir, 2004. **20**(22): p. 9868-9877.
79. Rudawska, A. and E. Jacniacka, *Analysis for determining surface free energy uncertainty by the Owen-Wendt method.* International Journal of Adhesion and Adhesives, 2009. **29**(4): p. 451-457.
80. Ratner, B.D., A. Chilkoti, and D.G. Castner, *Contemporary methods for characterizing complex biomaterial surfaces.* CLMA</cja:jid> Clinical Materials, 1992. **11**(1): p. 25-36.
81. Gantenbein-Ritter, B., et al., *Confocal imaging protocols for live/dead staining in three-dimensional carriers,* in *Mammalian Cell Viability*. 2011, Springer. p. 127-140.
82. Owens, D.K. and R.C. Wendt, *Estimation of Surface Free Energy of Polymers.* Journal of Applied Polymer Science, 1969. **13**(8): p. 1741-&.
83. Krol, P., J.B. Lechowicz, and B. Krol, *Modelling the surface free energy parameters of polyurethane coats-part 1. Solvent-based coats obtained from linear polyurethane elastomers.* Colloid and Polymer Science, 2013. **291**(4): p. 1031-1047.
84. Rulison, C., *Two-component surface energy characterization as a predictor of wettability and dispersability.* KRUSS Application note AN213, 2000: p. 1-22.
85. Luo, R., et al., *Effect of surface tension on the measurement of surface energy components of asphalt binders using the Wilhelmy Plate Method.* Construction and Building Materials, 2015. **98**: p. 900-909.
86. Brissova, M., et al., *Evaluation of microcapsule permeability via inverse size exclusion chromatography.* Analytical Biochemistry, 1996. **242**(1): p. 104-111.
87. Kongdee, A., et al., *INVERSE SIZE EXCLUSION CHROMATOGRAPHY-A TECHNIQUE OF PORE CHARACTERISATION OF TEXTILE MATERIALS.* Lenzinger Berichte, 2003. **82**(96-101): p. 193.
88. de Vos, P., et al., *Multiscale requirements for bioencapsulation in medicine and biotechnology.* Biomaterials, 2009. **30**(13): p. 2559-2570.
89. Fundueanu, G., et al., *Physico-chemical characterization of Ca-alginate microparticles produced with different methods.* Biomaterials, 1999. **20**(15): p. 1427-1435.
90. Yao, Y. and A.M. Lenhoff, *Determination of pore size distributions of porous chromatographic adsorbents by inverse size-exclusion chromatography.* Journal of Chromatography A, 2004. **1037**(1-2): p. 273-282.
91. Horiike, K., et al., *Interpretation of the Stokes radius of macromolecules determined by gel filtration chromatography.* The Journal of Biochemistry, 1983. **93**(1): p. 99-106.

92. Dembczynski, R. and T. Jankowski, *Determination of pore diameter and molecular weight cut-off of hydrogel-membrane liquid-core capsules for immunoisolation.* Journal of Biomaterials Science, Polymer Edition, 2001. **12**(9): p. 1051-1058.
93. Thanos, C., B. Bintz, and D.F. Emerich, *Stability of alginate-polyornithine microcapsules is profoundly dependent on the site of transplantation*. Vol. 81. 2007. 1-11.
94. Bhujbal, S.V., et al., *Factors influencing the mechanical stability of alginate beads applicable for immunoisolation of mammalian cells.* Journal of the mechanical behavior of biomedical materials, 2014. **37**: p. 196-208.
95. Reis, R.L., et al., *Natural-based polymers for biomedical applications*. 2008: Elsevier.
96. Bumbrah, G.S. and R.M. Sharma, *Raman spectroscopy – Basic principle, instrumentation and selected applications for the characterization of drugs of abuse.* Egyptian Journal of Forensic Sciences, 2016. **6**(3): p. 209-215.
97. Settle, F.A., *Handbook of instrumental techniques for analytical chemistry*. 1997: Prentice Hall PTR.
98. Skoog, D.A., F.J. Holler, and S.R. Crouch, *Principles of instrumental analysis*. 2017: Cengage learning.
99. Kroneková, Z., et al., *Structural changes in alginate-based microspheres exposed to in vivo environment as revealed by confocal Raman microscopy.* Scientific reports, 2018. **8**(1): p. 1637.
100. Skelin, M., M. Rupnik, and A. Cencič, *Pancreatic beta cell lines and their applications in diabetes mellitus research.* ALTEX-Alternatives to animal experimentation, 2010. **27**(2): p. 105-113.
101. Ulrich, A.B., et al., *Pancreatic cell lines: a review.* Pancreas, 2002. **24**(2): p. 111-120.
102. Santerre, R.F., et al., *Insulin synthesis in a clonal cell line of simian virus 40-transformed hamster pancreatic beta cells.* Proceedings of the National Academy of Sciences, 1981. **78**(7): p. 4339-4343.
103. Efrat, S., et al., *Beta-cell lines derived from transgenic mice expressing a hybrid insulin gene-oncogene.* Proceedings of the National Academy of Sciences, 1988. **85**(23): p. 9037-9041.
104. Asfari, M., et al., *Establishment of 2-mercaptoethanol-dependent differentiated insulin-secreting cell lines.* Endocrinology, 1992. **130**(1): p. 167-178.
105. Miyazaki, J.-I., et al., *Establishment of a pancreatic β cell line that retains glucose-inducible insulin secretion: special reference to expression of glucose transporter isoforms.* Endocrinology, 1990. **127**(1): p. 126-132.
106. Louis, K.S. and A.C. Siegel, *Cell viability analysis using trypan blue: manual and automated methods*, in *Mammalian cell viability*. 2011, Springer. p. 7-12.
107. Riccardi, C. and I. Nicoletti, *Analysis of apoptosis by propidium iodide staining and flow cytometry.* Nature protocols, 2006. **1**(3): p. 1458.
108. Chuah, A.M., et al., *Preparation of uniformly sized alginate microspheres using the novel combined methods of microchannel emulsification and external gelation.* Colloids and Surfaces A: Physicochemical and Engineering Aspects, 2009. **351**(1-3): p. 9-17.
109. Simpliciano, C., et al., *Cross-linked alginate film pore size determination using atomic force microscopy and validation using diffusivity determinations.* Journal of Surface Engineered Materials and Advanced Technology, 2013. **3**(04): p. 1.
110. Manev, Z., et al., *Structural mechanical and gelling propertieS of alginate beadS.* Bulgarian Journal of Agricultural Science, 2013. **19**(4): p. 770-774.

111. Jin, L., et al., *Monitoring of swelling and degrading behavior of alginate beads using optical tweezers.* Power, 2009. **10**(13): p. 10-14.
112. Bajpai, S. and S. Sharma, *Investigation of swelling/degradation behaviour of alginate beads crosslinked with Ca2+ and Ba2+ ions.* Reactive and Functional Polymers, 2004. **59**(2): p. 129-140.
113. Maa, J.Y., et al., *Flow behavior, thixotropy and dynamical viscoelasticity of sodium alginate aqueous solutions.* Food Hydrocolloids, 2014. **38**: p. 119-128.
114. Storz, H., et al., *Viscoelastic properties of ultra-high viscosity alginates.* Rheologica Acta, 2010. **49**(2): p. 155-167.
115. Hoesli, C.A., et al., *Mammalian Cell Encapsulation in Alginate Beads Using a Simple Stirred Vessel.* Jove-Journal of Visualized Experiments, 2017(124).
116. Carpenter, A.E., et al., *CellProfiler: image analysis software for identifying and quantifying cell phenotypes.* Genome Biology, 2006. **7**(10).
117. Briššová, M., et al., *Control and measurement of permeability for design of microcapsule cell delivery system.* Journal of Biomedical Materials Research, 1998. **39**(1): p. 61-70.
118. Rausch, M.H., et al., *Density, Surface Tension, and Kinematic Viscosity of Hydrofluoroethers HFE-7000, HFE-7100, HFE-7200, HFE-7300, and HFE-7500.* Journal of Chemical and Engineering Data, 2015. **60**(12): p. 3759-3765.
119. Tension, S., *Solid surface energy data (SFE) for common polymers.* Avaliable online: http://www. surface-tension. de/solid-surface-energy. htm (acessed on 14 January 2013), 2017.
120. Sahlin, E., et al., *Fabrication of microchannel structures in fluorinated ethylene propylene.* Analytical chemistry, 2002. **74**(17): p. 4566-4569.
121. Muhidinov, Z.K., et al., *Effect of Temperature on the Intrinsic Viscosity and Conformation of Different Pectins.* Polymer Science Series A, 2010. **52**(12): p. 1257-1263.
122. Haug, A. and O. Smidsrod, *Determination of Intrinsic Viscosity of Alginates.* Acta Chemica Scandinavica, 1962. **16**(7): p. 1569-&.
123. Lucio, A.A., et al., *Spatiotemporal variation of endogenous cell-generated stresses within 3D multicellular spheroids.* Scientific reports, 2017. **7**(1): p. 12022.
124. Sugiura, S., et al., *Characterization of spontaneous transformation-based droplet formation during microchannel emulsification.* Journal of Physical Chemistry B, 2002. **106**(36): p. 9405-9409.
125. Gu, H., M.H.G. Duits, and F. Mugele, *Droplets Formation and Merging in Two-Phase Flow Microfluidics.* International Journal of Molecular Sciences, 2011. **12**(4): p. 2572-2597.
126. Xu, J.H., et al., *Correlations of droplet formation in T-junction microfluidic devices: from squeezing to dripping.* Microfluidics and Nanofluidics, 2008. **5**(6): p. 711-717.
127. Vladisavljevic, G.T., I. Kobayashi, and M. Nakajima, *Effect of dispersed phase viscosity on maximum droplet generation frequency in microchannel emulsification using asymmetric straight-through channels.* Microfluidics and Nanofluidics, 2011. **10**(6): p. 1199-1209.
128. Kukizaki, M., *Shirasu porous glass (SPG) membrane emulsification in the absence of shear flow at the membrane surface: Influence of surfactant type and concentration, viscosities of dispersed and continuous phases, and transmembrane pressure.* Journal of Membrane Science, 2009. **327**(1): p. 234-243.

129. Thanos, C.G., B.E. Bintz, and D.F. Emerich, *Stability of alginate-polyornithine microcapsules is profoundly dependent on the site of transplantation.* Journal of Biomedical Materials Research Part A, 2007. **81a**(1): p. 1-11.
130. Thanos, C., et al., *Formulating the alginate–polyornithine biocapsule for prolonged stability: Evaluation of composition and manufacturing technique.* Journal of Biomedical Materials Research Part A: An Official Journal of The Society for Biomaterials, The Japanese Society for Biomaterials, and The Australian Society for Biomaterials and the Korean Society for Biomaterials, 2007. **83**(1): p. 216-224.
131. Qi, M.R.G., et al., *Survival of human islets in microbeads containing high guluronic acid alginate crosslinked with Ca2+ and Ba2+*. Xenotransplantation, 2012. **19**(6): p. 355-364.
132. Cui, H., et al., *Long-term metabolic control of autoimmune diabetes in spontaneously diabetic nonobese diabetic mice by nonvascularized microencapsulated adult porcine islets.* Transplantation, 2009. **88**(2): p. 160-169.
133. Schneider, S., et al., *Long-term graft function of adult rat and human islets encapsulated in novel alginate-based microcapsules after transplantation in immunocompetent diabetic mice.* Diabetes, 2005. **54**(3): p. 687-693.
134. Mørch, Ý.A., et al., *Effect of Ca2+, Ba2+, and Sr2+ on alginate microbeads.* Biomacromolecules, 2006. **7**(5): p. 1471-1480.
135. Mørch, Y.A., et al., *Binding and Leakage of Barium in Alginate Microbeads.* Journal of biomedical materials research. Part A, 2012. **100**(11): p. 2939-2947.
136. Krasaekoopt, W., B. Bhandari, and H. Deeth, *The influence of coating materials on some properties of alginate beads and survivability of microencapsulated probiotic bacteria.* International Dairy Journal, 2004. **14**(8): p. 737-743.
137. de Vos, P., et al., *Zeta-potentials of alginate-PLL capsules: A predictive measure for biocompatibility?* Journal of biomedical materials research Part A, 2007. **80**(4): p. 813-819.
138. Whelehan, M. and I. Marison, *Microencapsulation using vibrating technology*. Vol. 28. 2011. 669-88.
139. Poncelet, D., et al., *A Parallel plate electrostatic droplet generator: Parameters affecting microbead size.* Applied Microbiology and Biotechnology, 1994. **42**(2): p. 251-255.
140. Van Dijke, K.C., K.C. Schroën, and R.M. Boom, *Microchannel emulsification: from computational fluid dynamics to predictive analytical model.* Langmuir, 2008. **24**(18): p. 10107-10115.
141. F. Gibbs, S.K., Inteaz Alli, Catherine N. Mulligan, Bernard, *Encapsulation in the food industry: a review.* International journal of food sciences and nutrition, 1999. **50**(3): p. 213-224.
142. Gonzalez-Arnao, M.T. and F. Engelmann, *Cryopreservation of plant germplasm using the encapsulation-dehydration technique: review and case study on sugarcane.* CryoLetters, 2006. **27**(3): p. 155-168.
143. Strand, B.L., A.E. Coron, and G. Skjak-Braek, *Current and future perspectives on alginate encapsulated pancreatic islet.* Stem cells translational medicine, 2017. **6**(4): p. 1053-1058.
144. Shilpa, A., S. Agrawal, and A.R. Ray, *Controlled delivery of drugs from alginate matrix.* Journal of Macromolecular Science, Part C: Polymer Reviews, 2003. **43**(2): p. 187-221.
145. de Vos, P., et al., *Encapsulation for preservation of functionality and targeted delivery of bioactive food components.* International Dairy Journal, 2010. **20**(4): p. 292-302.

146. Cahill, S., M. Upton, and A. McLoughlin, *Bioencapsulation technology in meat preservation*, in *Applied Microbiology*. 2001, Springer. p. 239-266.
147. Casanova, F. and L. Santos, *Encapsulation of cosmetic active ingredients for topical application–a review*. Journal of microencapsulation, 2016. **33**(1): p. 1-17.

10 Appendices

10.1 Supplementary Figures

The correlation between the alginate concentration and the measured alginate solution density is displayed in Figure 22. The trend was found to be statistically insignificant. Therefore, there is little to no change in the density of the alginate phase with increasing alginate concentration.

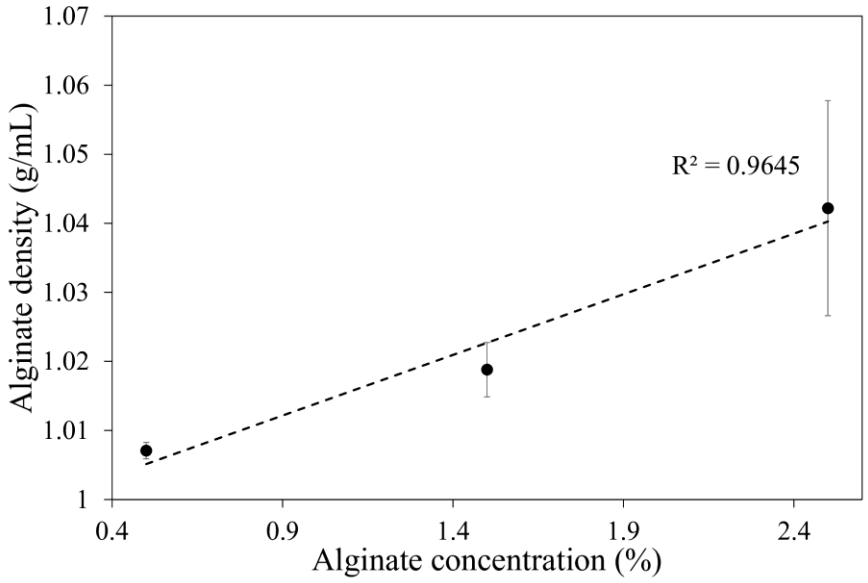

Figure 22. Effect of alginate concentration on the measured fluid density.
Statistically insignificant effect with p = 0.09. Error bars represent standard error of n=3 runs.

10.2 Supplementary Tables

The data of the 2^2 full factorial experiment with three center point runs and two replicates is summarized in Table 7.

Table 7. Full factorial experimental design and raw data for determining the significance of the effects of alginate concentration and flow rate on the average diameter of microbeads generated via microchannel emulsification.
Statistically significant effect of alginate concentration on microbead diameter with $p < 0.01$. Statistically insignificant effect of flow rate and the interaction of flow rate and concentration on microbead diameter with $p = 0.30$ and 0.41, respectively.

Alginate Concentration (%)	Alginate Flow Rate (mL/min)	Average Microbead Diameter (mm)	Microbead Coefficient of Variation (%)
1.5	0.55	1.893	7.8
2.5	0.31	1.886	10.0
0.5	0.78	1.548	9.1
1.5	0.55	2.230	3.0
2.5	0.78	2.876	10.9
1.5	0.55	2.055	11.7
0.5	0.31	1.599	23.8
1.5	0.55	1.869	9.17
0.5	0.31	1.812	12.8
2.5	0.78	2.167	7.14
1.5	0.55	1.858	8.1
0.5	0.78	1.948	17.9
1.5	0.55	1.933	10.2
2.5	0.31	2.453	10.5

10.3 Sample Calculations

Shear rate in microchannels

First, the velocity (v) of alginate fluid flowing through 700 µm x 200 µm microchannels at a flow rate of 0.55 mL/min was approximated as follows:

$$v = \frac{0.55\,\frac{mL}{min} * \frac{10^{12}\mu m^3}{mL} * \frac{1\,min}{60\,s}}{700\,\mu m * 200\,\mu m} = 6.55 * 10^4\,\frac{\mu m}{s}$$

Next, the hydraulic radius of the rectangular microchannels (h) is determined:

$$h = \frac{hydraulic\ diameter}{2} = \frac{2A}{P} = \frac{2 * 700\,\mu m * 200\,\mu m}{2 * (700\,\mu m + 200\,\mu m)} = 156\ \mu m$$

The minimum shear rate ($\dot{\gamma}$) in the microchannel can therefore be calculated as follows:

$$\dot{\gamma} = \frac{v}{h} = \frac{6.55*10^4 \frac{\mu m}{s}}{156\,\mu m} = 420\ s^{-1}$$

Critical capillary number

The viscosity of a 1.5% alginate fluid at 25ºC flowing through the microchannel assuming a shear rate of 420 s^{-1} can be determined using the cross model:

$$\eta = \eta_\infty + \frac{\eta_0 - \eta_\infty}{1 + (K_c\dot{\gamma})^m} = 0.039\ Pa \cdot s + \frac{0.14\ Pa{\cdot}s - 0.039\ Pa{\cdot}s}{1 + (117.8\ s * 420\ s^{-1})^{0.378}} = 0.041\ Pa \cdot s$$

The alginate velocity (U) through a 700 µm x 200 µm microchannel is calculated at the experimental alginate flow rate at first transition (F_1):

$$U = \frac{F_1}{0.07\ cm * 0.02\ cm} = \frac{3.45\ \pm 0.32\ cm^3/min}{0.07\ cm * 0.02\ cm} = 0.41\ \pm 0.04\,\frac{m}{s}$$

The approximate critical capillary number can then be calculated as follows:

$$Ca = \frac{\eta_d U}{\gamma_{eq}} = \frac{(0.041\ Pa \cdot s)(0.41\ \pm 0.04\ m/s)}{43\,\frac{mN}{m}\left(\frac{1\ N}{1000\ mN}\right)} = 0.39 \pm 0.04$$